https://doi.org/10.5194/egusphere-2026-4398
Preprint. Discussion started: 6 August 2026

Phytoplankton size structure in the northwestern Weddell Sea

Robert J.W. Brewin [1,★], Bethany Wilkinson [2,★], Xuerong Sun [1,★], Giorgio Dall'Olmo [3], Gavin H. Tilstone [2], Katharine R. Hendry [4], Sarah Breimann [2], Ian Brown [2], Angus Atkinson [2], Katrin Schmidt [5], Elisabetta Canuti [6], Meredith G. Meyer [7], Qi Zheng [1], Johannes J. Viljoen [1], Tom Bell [2], and Karen J. Heywood [7]

[1]Centre for Geography and Environmental Science, Department of Earth and Environmental Sciences, Faculty of Environment, Science and Economy, University of Exeter, Cornwall, UK
[2]Plymouth Marine Laboratory, Plymouth, UK
[3]Istituto Nazionale di Oceanografia e di Geofisica Sperimentale, Trieste, Italy
[4]British Antarctic Survey, Cambridge, UK
[5]School of Geography, Earth and Environmental Sciences, Faculty of Science and Engineering, University of Plymouth, UK
[6]European Commission, Joint Research Centre (JRC), Ispra, Italy
[7]Centre for Ocean and Atmospheric Sciences, School of Environmental Sciences, University of East Anglia, Norwich, UK
★These authors contributed equally to this work.

Correspondence: Robert J.W. Brewin (r.brewin@exeter.ac.uk)

Abstract. The size of phytoplankton is a key metric that influences organic carbon production in the ocean and its transfer efficiency through marine foodwebs. There is evidence that the size structure of phytoplankton in Antarctic waters differs markedly from that in tropical oceans. However, logistical challenges have left many Antarctic regions poorly sampled. Here, we explore a dataset collected during an austral summer research cruise to the rarely sampled northwestern Weddell Sea continental shelf and open waters, near the eastern Antarctic Peninsula. The dataset includes discrete measurements of size-fractionated chlorophyll-*a* concentration (pico- $<2\,\mu$m, nano- 2-20 μm, and micro-phytoplankton $>20\,\mu$m) obtained using *in-vitro* fluorescence and sequential size-fractionated filtration (SFF), phytoplankton pigments measured by high performance liquid chromatography (HPLC), and *in-situ* radiometric (ocean-colour) observations. We find broad agreement between HPLC-based (using diagnostic pigment analysis) and SFF-based estimates of total and size-fractionated chlorophyll-*a*, but with systematic differences for some size classes depending on the technique used. Ocean-colour chlorophyll-*a* algorithms developed in other regions of the Southern Ocean perform well in the northwestern Weddell Sea and outperform standard global algorithms, which systematically underestimate chlorophyll-*a*. SFF measurements indicate that medium sized phytoplankton (nanophytoplankton) dominate both shelf and open waters of the northwestern Weddell Sea. We fitted a simple three-component model to the SFF data describing the partitioning of chlorophyll-*a* among the three size classes as a function of total chlorophyll-*a*. Model parameters were similar to those derived from an independent dataset from the western Antarctic Peninsula, supporting the broader dominance of nanophytoplankton around the entire Antarctic Peninsula, but differed markedly from parameters derived from lower latitude tropical and subtropical (50°N to 50°S) Atlantic waters, where picophytoplankton dominate. Finally, we combined satellite-derived estimates of total chlorophyll-*a* during the cruise period with the tuned model parameters to map the spatial distribution of phytoplankton size classes across the broader northwestern Weddell Sea region, which confirmed the

https://doi.org/10.5194/egusphere-2026-4398
Preprint. Discussion started: 6 August 2026

widespread dominance of nanophytoplankton. These datasets provide a valuable baseline for quantifying the rate and fate of organic carbon production in this rapidly changing region.

1 Introduction

Existing at the base of the marine food web, phytoplankton channel energy from the sun into the production of organic carbon, through the process of photosynthesis. They produce as much oxygen and organic carbon as terrestrial plants do on land (Longhurst et al., 1995; Field et al., 1998) and help regulate atmospheric carbon through their contribution to the ocean's biological carbon pump (Sanders et al., 2014; Brewin et al., 2021; Nowicki et al., 2022). Quantifying phytoplankton biomass is required to study spatial and temporal changes in phytoplankton, and a common proxy used for this is the total chlorophyll-*a* concentration (Chl-*a*). Although Chl-*a* can change independently of carbon biomass, through processes like photo-acclimation (Laws and Bannister, 1980), it is present in all phytoplankton (though sometimes varying in Chl-*a* type) and is easy to measure *in situ* and remotely (Sathyendranath et al., 2023). It has consequently been included in the list of Essential Climate Variables by the Global Climate Observing System (GCOS, 2011).

Another important characteristic of phytoplankton is their size structure (Marañón, 2009). Phytoplankton size is a master trait (Marañón, 2015), influencing physiology, metabolic rates, nutrient uptake, and light absorption (Chisholm, 1992; Uitz et al., 2008; Brewin et al., 2019a). There is also evidence of preferential size-based feeding by zooplankton (Fuchs and Franks, 2010; Kiørboe, 2011), suggesting that size structure regulates trophic interactions and energy transfer through the food web (Maloney and Field, 1991; Legendre and LeFevre, 1991; Parsons and Lalli, 2002), as well as the export of organic carbon to the ocean interior (Guidi et al., 2009). A size-based partitioning of phytoplankton biomass (Chl-*a*) has been recognised as a key ecological indicator (Platt and Sathyendranath, 2008) and underpins the structure of many large-scale marine biogeochemical models (Aumont et al., 2003; Kishi et al., 2007; Marinov et al., 2010; Ward et al., 2012; Butenschön et al., 2016). Chl-*a* is often partitioned into three key size classes: pico- ($<2\,\mu$m), nano- (2-20 μm), and micro-phytoplankton ($>20\,\mu$m) (Sieburth et al., 1978), that are thought to play key functions in the cycling of organic carbon in the ocean (IOCCG, 2014).

Although advanced methods for quantifying Chl-*a* in these size classes are emerging (e.g., automated quantitative cell imagery combined with conventional flow cytometry, see Chase et al., 2020), the two most common methods used at sea are size-fractionated filtration (SFF) and diagnostic pigment analysis (DPA) on high performance liquid chromatography (HPLC) quantified pigment composition (Brewin et al., 2014a). SFF involves filtering seawater sequentially through a series of filters, typically polycarbonate membranes with nominal pore sizes of 20, 2, and 0.2 μm, under low vacuum pressure. Chl-*a* retained on each filter is extracted in solvent and quantified using a calibrated bench-top fluorometer. The principal advantage of this approach is that it directly partitions Chl-*a* among three phytoplankton size classes. However, uncertainties can arise from inaccuracies in nominal pore size, retention of particles smaller than the stated pore diameter, cell breakage during filtration, and the complex morphology of some phytoplankton taxa (Sheldon, 1972; Logan, 1993; Logan et al., 1994; Droppo, 2000; Knefelkamp et al., 2007; Dall'Olmo et al., 2009). The DPA method involves filtering seawater, typically onto a glass-fibre filter with a nominal pore size of 0.7 μm, extracting the retained pigments in solvent, and quantifying Chl-*a* and seven diagnostic

https://doi.org/10.5194/egusphere-2026-4398
Preprint. Discussion started: 6 August 2026

pigments using HPLC (Claustre, 1994; Vidussi et al., 2001). These pigments are then used in a multilinear regression to reconstruct Chl-*a* and estimate its partitioning among three phytoplankton size classes (Uitz et al., 2006). Like SFF, DPA covers the three phytoplankton size classes, but because DPA infers size structure from pigment composition rather than physically separating size classes, it is less affected by artefacts associated with sequential filtration, such as cell breakage. However, DPA does not provide a direct measure of cell size. Pigments considered diagnostic of particular size classes can occur in multiple taxa and size ranges, and accessory pigment composition can vary independently of size, in response to environmental conditions such as light and nutrient availability (Uitz et al., 2009; Brewin et al., 2014a; Chase et al., 2020). Despite these limitations, SFF and HPLC-based DPA remain the most widely used approaches for quantifying phytoplankton size structure, and large datasets have been compiled to examine global patterns in size distribution (e.g., Sun et al., 2023, 2025b).

SFF and DPA data compilations have revealed clear macroecological patterns in phytoplankton size structure, with smaller phytoplankton generally associated with low concentrations of Chl-*a* and large cells increasingly dominant at higher concentrations (Uitz et al., 2006; Sun et al., 2023). Brewin et al. (2010) developed a simple conceptual four-parameter model that captures these broad patterns, and has been widely used to study how they vary at regional scales (e.g., Brewin et al., 2012; Brotas et al., 2013; Lin et al., 2014; Brito et al., 2015; Sammartino et al., 2015; Ward, 2015; Sahay et al., 2017; Corredor-Acosta et al., 2018; Lamont et al., 2018b; Brewin et al., 2019b; Sun et al., 2019; Gittings et al., 2025). This approach has also proven useful for mapping the size classes of phytoplankton using satellite-derived Chl-*a* as model input (e.g. Brewin et al., 2015; Lamont et al., 2018a). One region where patterns appear to differ is the Southern Ocean, with a greater presence of larger phytoplankton (nano- and micro-phytoplankton) seen over the full Chl-*a* range when compared with tropical waters (Ward, 2015; Sun et al., 2023, 2025a). These differences may help explain regional variability in marine organic carbon cycling (Boyd et al., 2024) and the requirement for regional ocean colour Chl-*a* algorithms (Sun et al., 2025a).

The seas around Antarctica are among the most remote waters on Earth, and many regions are not well sampled. Over the past decade, they have been warming (Wille et al., 2024), freshening (Naughten et al., 2023) and losing sea ice (Purich and Doddridge, 2023), with implications for ecosystem dynamics (Deppeler and Davidson, 2017; Atkinson et al., 2022, 2025; Mendes et al., 2023; Soja-Woźniak et al., 2025; Abram et al., 2025; Hayward et al., 2025). Unlike the western Antarctic Peninsula, where long-term monitoring programmes have been established for decades (Smith et al., 1995; Venables et al., 2023) and where phytoplankton size structure has been extensively studied (Weber and El-Sayed, 1987; Savidge et al., 1995; Garibotti et al., 2003; Montes-Hugo et al., 2008; Hewes, 2009; García-Muñoz et al., 2014; Gonçalves-Araujo et al., 2015; Biggs et al., 2019), the eastern Antarctic Peninsula and the northwestern Weddell Sea continental shelf remain markedly undersampled. Most phytoplankton size-structure studies in the wider Weddell Sea region have concentrated either in the eastern sector (von Bröckel, 1985; Laubscher et al., 1993; Dower et al., 1996; Froneman et al., 2004; Flynn et al., 2023) or in more northern marginal ice zone environments (Jacques and Panouse, 1991; Becquevort et al., 1992; Lancelot et al., 1993; Jochem et al., 1995; Clarke and Leakey, 1996; Xiuren et al., 1996; Ward et al., 2006; Vernet et al., 2011).

Here, we present a dataset of SFF, HPLC-DPA, and ocean-colour radiometric measurements collected during a research cruise to the northwestern Weddell Sea continental shelf near the eastern Antarctic Peninsula, as part of the Processes Influencing Carbon Cycling: Observations of the Lower limb of the Antarctic Overturning (PICCOLO) programme (Heywood and

https://doi.org/10.5194/egusphere-2026-4398
Preprint. Discussion started: 6 August 2026

Bell, 2024). We use these observations to characterise phytoplankton size structure in this undersampled region and address four questions: (1) How do DPA and SFF estimates of size-fractionated Chl-*a* compare? (2) How well do satellite Chl-*a* algorithms perform? (3) Which size class of phytoplankton dominate Chl-*a*? (4) Do regional size-structure patterns in the eastern Antarctic Peninsula resemble those of the western Antarctic Peninsula and diverge from temperate and subtropical oceans?

2 Methods

2.1 Study area

The PICCOLO cruise (SDA035) sampled waters across the continental shelf of the eastern Antarctic Peninsula and the open waters of the northwestern Weddell Sea (Figure 1). Conducted aboard the *RRS* Sir David Attenborough, the expedition encompassed a wide range of oceanographic regimes, extending as far south as the Larsen C Ice Shelf. The sampling strategy included a transect from the deep open ocean across the continental slope and shelf, capturing gradients in physical and biogeochemical conditions. Water samples were collected primarily using a CTD rosette supplemented by samples from the ship's underway surface seawater system. Data were categorised into open water samples collected during a transect onto the shelf (>500 m), shelf samples (<500 m), and those collected near the Larsen C ice shelf (Figure 1).

2.2 Size-fractionated filtration (SFF) data

2.2.1 PICCOLO SFF data

Water samples were collected from CTD casts at depths corresponding to approximately 0.1%, 1%, 4.5%, 14%, and 33% of surface irradiance (20-202 m), and near-surface waters (typically <20 m). Samples were drawn into bottles wrapped in black tape to minimize light exposure. Approximately 100 mL of seawater was filtered directly (no pre-filtration) under low vacuum pressure through a sequential series of polycarbonate filters with pore sizes of 20μm, 2μm and 0.1μm. Following filtration, each filter was placed in a 15 mL Falcon tube and stored at $-80\,^{\circ}\mathrm{C}$ until analysis. Pigments were extracted by adding 10 mL of 90% aqueous acetone to each tube and incubating the samples for up to 24 h at $-20\,^{\circ}\mathrm{C}$. After extraction, the samples were allowed to equilibrate to room temperature in the dark for at least 1 h. Raw fluorescence (RFU) was measured using a Turner Trilogy fluorometer and converted to Chl-*a* concentrations (mg m^{-3}) using a calibration based on Chl-*a* standards.

Size-fractionated Chl-*a* were defined according to the sequential filtration scheme. Picophytoplankton chlorophyll (<2 μm) was quantified as the Chl-*a* passing through the 2 μm filter and retained on the 0.1 μm filter. Nanophytoplankton chlorophyll (2–20 μm) was defined as the Chl-*a* passing through the 20 μm filter and retained on the 2 μm filter. Microphytoplankton chlorophyll (>20 μm) corresponded to the Chl-*a* retained on the 20 μm filter. The combined pico- and nanophytoplankton Chl-*a* (<20 μm) was calculated as the Chl-*a* passing through the 20 μm filter and retained on either the 2 μm or 0.1 μm filters. Total size-fractionated Chl-*a* was calculated as the sum of the pico-, nano-, and micro-phytoplankton Chl-*a* for each sample. Additional details on the PICCOLO SFF data are provided in Table 1 and in Wilkinson (2026). The location of samples are shown in Figure 1.

https://doi.org/10.5194/egusphere-2026-4398
Preprint. Discussion started: 6 August 2026

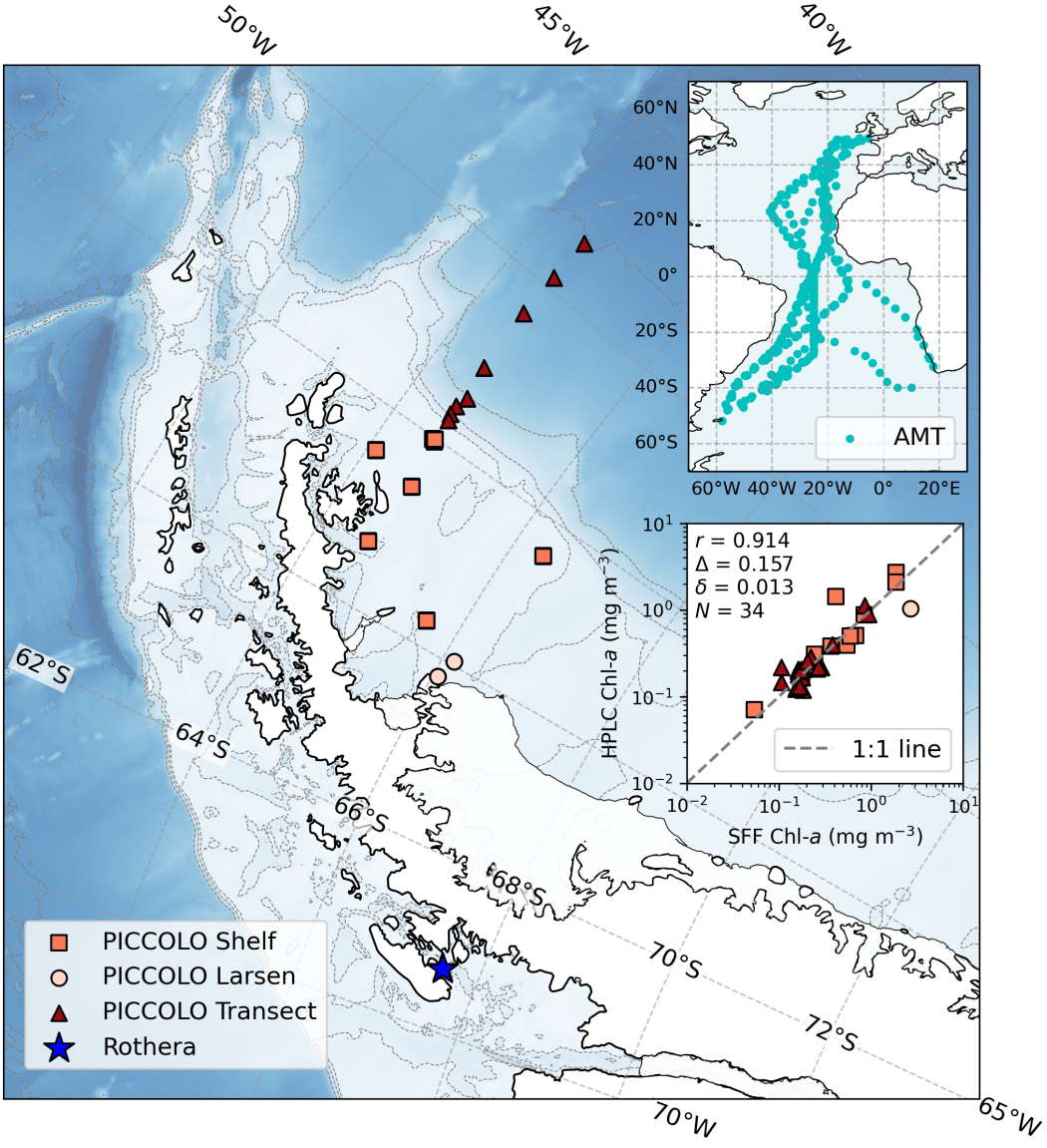

Figure 1. Map of study site and locations of data used in the study. Background shading represent IBCSO bathymetry (Dorschel et al., 2022) with contours at 500, 1000, 2000, and 4000 m. An ice shelf layer is overlain onto the map in transparent white, taken from the Scientific Committee on Antarctic Research (https://www.add.scar.org/), to illustrate the position of the Larsen and George VI ice shelves. Upper inset figure shows locations of AMT data. Lower inset figure shows a scatter plot of total Chl-*a* between matched HPLC and SFF data on the PICCOLO cruise. r is the correlation coefficient, Δ the unbiased root mean square error and δ the bias. Statistics were performed on $\log_{10}$-transformed Chl-*a*.

https://doi.org/10.5194/egusphere-2026-4398
Preprint. Discussion started: 6 August 2026

Table 1. Summary of datasets used in this study.

Dataset	Type	Time (month/year)	Location	Number of obs.	Depth range (m)
PICCOLO	SFF	01/2024 – 03/2024	northwestern Weddell Sea	133	0–202
PICCOLO	HPLC	01/2024 – 03/2024	northwestern Weddell Sea	34*	0–80
PICCOLO	R_{rs}	01/2024 – 03/2024	northwestern Weddell Sea	13* (24$)	above water
Rothera	SFF	02/1997 – 12/2017	western Antarctic Peninsula	742	15
AMT	SFF	04/1996 – 11/2013	Atlantic Ocean	1501	0–240

* Number of observations that match the PICCOLO SFF dataset.

$ Number of observations that match the PICCOLO HPLC dataset.

2.2.2 Rothera Research Station SFF data

A long-term year round dataset (1997-2017) of size-fractionated Chl-*a* from Ryder Bay, West Antarctic Peninsula, near Rothera Research Stations as part of the Rothera Oceanographic and Biological Time Series (RaTS) (Figure 1) was utilised in this work for comparison with PICCOLO data. Details of the dataset are provided by Venables et al. (2023) and Clarke et al. (2022), and are briefly described here. Water was sampled from 15 m depth using a Niskin bottle and transferred to the Bonner Laboratory at Rothera for analysis. Water samples were gently mixed by inversion and, immediately upon return to the research station, filtered in triplicate by gravity through a series of 47 mm membrane filters. Filtration volumes were adjusted according to expected Chl-*a* concentrations: 100 mL per replicate in the austral summer (higher productivity, more turbid) and 500 mL per replicate in the austral winter (lower productivity, less turbid).

Sequential filtration separated the phytoplankton community into four size fractions: microphytoplankton (>20 μm), collected using nylon mesh; large nanophytoplankton (5–20 μm), retained on the 5 μm membrane filter having passed through the 20 μm nylon mesh; small nanophytoplankton (2–5 μm), retained on the 2 μm membrane filter have passed through the 5 μm membrane filter and the 20 μm nylon mesh, and picophytoplankton (0.2–2 μm), retained on the 0.2 μm membrane filter, having passed through the 20 μm nylon mesh and the 5 μm and 2 μm membrane filter. Chl-*a* was extracted in chloroform or methanol and measured fluorometrically using a calibrated Turner AU-10 fluorometer. This was done before and after acidification with two drops of 0.1 Normal Hydrochloric Acid under low light, to remove the contribution of phaeopigment. The large and small nanophytoplankton Chl-*a* were summed to compute nanophytoplankton Chl-*a* (2–20 μm), consistent with PICCOLO. Quality control was performed on Chl-*a* measurements: records with total Chl-*a* < 0.001 were removed, and any total or size-fractionated Chl-*a* values that were blank, negative, equal to 0.001, or ≤ 0.0001 were excluded. Records with comments indicating unsuccessful sample collection were also removed. The number of records decreased from 890 to 742. Additional details on the Rothera SFF data are provided in Table 1.

https://doi.org/10.5194/egusphere-2026-4398
Preprint. Discussion started: 6 August 2026

2.2.3 AMT SFF data

A dataset of SFF collected on Atlantic Meridional Transects (AMT) between 1996 and 2013 was used in the study for comparison with PICCOLO SFF data (Figure 1). The dataset was compiled from Sun et al. (2023), collected on AMT cruises 2, 3, 4, 5, 6, 11, 13, 14, 15, 19, 22 and 23. Details of the methods are provided by Brewin et al. (2014a, b, 2017b), Tilstone et al. (2017) and Sun et al. (2023). In general, methods were very similar to PICCOLO. Between ∼200-300 ml of water were sequentially filtered through different-sized polycarbonate filters. All cruises included 2 μm and 0.2 μm pore size filters, AMT cruises 2, 3, 4, 5, 6 and 11 used in addition 20 μm filters, with cruises 13, 14, 22 and 23, using in addition 10 μm and/or 5 μm pore size filters. Following filtration, pigments were extracted by storing filters in 90% acetone at $-20\,^{\circ}$C for 10–24 h. Chl-*a* were then determined fluorometrically using a Turner Designs 10-AU Fluorometer, Turner Designs TD-700 Fluorometer, or Turner Designs Trilogy Laboratory Fluorometer, depending on the cruise. For each cruise, the fluorometer was calibrated before and after analysis using pure chlorophyll a standards. Total Chl-*a* was quantified as the sum of all fractions. To be consistent with PICCOLO SFF data, only measurements of size-fractionated Chl-*a* for pico- <2 μm, nano- 2-20 μm, and micro-phytoplankton >20 μm were used. Additional details on the AMT SFF data are provided in Table 1.

2.2.4 Three-component model

To compare macroecological patterns in phytoplankton size structure among the three SFF datasets, we adopted the three-component model of Brewin et al. (2010, 2015). The model uses two exponential functions where the fraction of combined pico- and nanoplankton (denoted $F_{p,n}$, cells <20 μm) and picoplankton (denoted F_p, cells <2 μm) to total Chl-*a* (C) are expressed as

$$F_{p,n} = C^m_{p,n}[1 - \exp(-\frac{D_{p,n}}{C^m_{p,n}}C)]/C, \tag{1}$$

and

$$F_p = C^m_p[1 - \exp(-\frac{D_p}{C^m_p}C)]/C. \tag{2}$$

$C^m_{p,n}$ and C^m_p represent the asymptotic maximum values for the two size classes (<20 μm and <2 μm respectively) and $D_{p,n}$ and D_p reflect the fraction of each size-class (<20 μm and <2 μm respectively) to total Chl-*a* as it tends to zero. The fraction of nano-phytoplankton (F_n) micro-phytoplankton (F_m) to Chl-*a* can then be calculated according to

$$F_n = F_{p,n} - F_p, \tag{3}$$

and

$$F_m = 1 - C_{p,n}. \tag{4}$$

The Chl-*a* concentration of each size class (C_p, C_n and C_m) can be then be calculated by multiplying the fractions by the total Chl-*a* (C). The model (Eq. 1 and 2) was fitted to SFF data separately for the three datasets (PICCOLO, Rothera and AMT)

https://doi.org/10.5194/egusphere-2026-4398
Preprint. Discussion started: 6 August 2026

to derived a set of parameters for each dataset ($C^m_{p,n}$, C^m_p, $D_{p,n}$ and D_p) using a standard, nonlinear least-squares method (Levenberg-Marquardt, Python function *lmfit*) that can quantify uncertainties in model parameters from the covariance matrix of the fit.

2.3 High performance liquid chromatography (HPLC) diagnostic pigment analysis (DPA)

A dataset of HPLC pigments collected on PICCOLO was utilised in this work. Details of the method used are provided by Meyer et al. (2026a) and briefly summarised here. Water samples were collected from the ship's underway seawater system (intake depth ∼7 m) and from discrete depths from CTD casts. Between 360 and 2000 mL of seawater was filtered onto 25 mm Whatman GF/F filters (0.7μm nominal pore size) under low vacuum, then flash-frozen in liquid nitrogen and stored at $-80\,^{\circ}$C until analysis. Pigment analyses were conducted by either DHI Analytics, following the HPLC method of Van Heukelem and Thomas (2001), or by the European Commission Joint Research Centre, also following the methods of Van Heukelem and Thomas (2001) as implemented by Canuti (2023). We did not use any prefiltered or sea ice samples in this analysis. Only HPLC measurements matched with either SFF data (see Section 2.2.1) or ocean colour data (see Section 2.4.1), were utilised in this work. For a more complete description of the PICCOLO HPLC dataset the reader is referred to Meyer et al. (2026a, b). Additional details on the HPLC data used in this study are provided in Table 1.

DPA analysis was used to estimate the fractions of pico- (F_p), nano- (F_n) and micro-phytoplankton (F_m) in the total chlorophyll concentration from the HPLC data (Vidussi et al., 2001; Uitz et al., 2006). This involved computing the total Chl-*a* (C) concentration (MV chlorophyll-*a* plus DV chlorophyll-*a* and Chlorophyllide-*a* where available) and seven diagnostic pigments: fucoxanthin, peridinin, 19'-hexanoyloxyfucoxanthin, 19'-butanoyloxyfucoxanthin, alloxanthin, chlorophyll-b and zeaxanthin. Firstly, the total chlorophyll concentration is reconstructed the weighted sum of the seven diagnostic pigments (denoted C_w), according to

$$C_w = \sum_{i=1}^{7} W_i P_i, \tag{5}$$

where the pigments are [**P**] = {fucoxanthin; peridinin; 19'-hexanoyloxyfucoxanthin; 19'-butanoyloxyfucoxanthin; alloxanthin; chlorophyll-b and divinyl chlorophyll-b; zeaxanthin} (note the the order in which the pigments are reported here is important for the equations later). Four DPA methods were used, each with a different set of weights: Uitz et al. (2006) where the weights [**W**] = {1.41; 1.41; 1.27; 0.35; 0.60; 1.01; 0.86}; Chase et al. (2020) where [**W**] = {2.62; 1.32; 0.87; 0.00; 2.64; 0.94; 1.52}; Sun et al. (2023) from a global complication of data [**W**] = {1.74; 1.52; 1.24; 0.55; 1.76; 1.78; 1.04}; and Sun et al. (2025a) from a complication of data in the Southern Ocean [**W**] = {1.30; 0.91; 1.02; 0.82; 1.60; 1.31; 1.30}.

2.3.1 Uitz et al. (2006) DPA size fractions

For the Uitz et al. (2006) DPA method the fractions of Chl-*a* in each size classes are derived according to

$$F_m = \frac{\sum_{i=1}^{2} W_i P_i}{C_w}, \tag{6}$$

https://doi.org/10.5194/egusphere-2026-4398
Preprint. Discussion started: 6 August 2026

$$F_n = \frac{\sum_{i=3}^{5} W_i P_i}{C_w}, \tag{7}$$

and

$$F_p = \frac{\sum_{i=6}^{7} W_i P_i}{C_w}. \tag{8}$$

2.3.2 Chase et al. (2020) DPA size fractions

For the Chase et al. (2020) DPA method, the fractions of Chl-*a* in each size classes are derived according to

$$F_m = \frac{0.5W_1P_1 + 0.25W_2P_2}{C_w}, \tag{9}$$

$$F_n = \frac{0.5W_1P_1 + 0.75W_2P_2 + \sum_{i=3}^{5} W_i P_i + 0.5W_6P_6}{C_w}, \tag{10}$$

and

$$F_p = \frac{0.5W_6P_6 + W_7P_7}{C_w}. \tag{11}$$

2.3.3 Sun et al. (2023, 2025a) DPA size fractions

The Sun et al. (2023) and Sun et al. (2025a) DPA methods are technically the same, albeit with different set of coefficients for the fucoxanthin adjustment of Devred et al. (2011), as well as for the weights described previously. The method first requires estimating a portion of the fucoxanthin pigment (P_1) in the nanoplankton pool ($P_{1,n}$), for example, from nano-sized diatoms. This is estimated according to

$$P_{1,n} = 10^{q_1 \log_{10}(P_3) + q_2 \log_{10}(P_4)}, \tag{12}$$

where P_3 and P_4 are to 19'-hexanoyloxyfucoxanthin and 19'-butanoyloxyfucoxanthin, and coefficients q_1 and q_2 are tuned, with Sun et al. (2023) $q_1 = 0.31$ and $q_2 = 1.16$, and Sun et al. (2025a) $q_1 = 0.20$ and $q_2 = 0.85$. The fucoxanthin concentration associated with microplankton ($P_{1,m}$) can be computed from $P_{1,m} = P_1 - P_{1,n}$ (NB: any cases where $P_{1,m}$ was negative, $P_{1,m} = 0$ and $P_{1,n} = P_1$). The fractions of chlorophyll in each size classes are then derived according to

$$F_m = \frac{\sum_{i=1}^{2} W_i P_i - W_1 P_{1,n}}{C_w}, \tag{13}$$

$$F_n = \begin{cases} \frac{12.5CW_3P_3}{C_w} + \frac{\sum_{i=4}^{5} W_i P_i + W_1 P_{1,n}}{C_w} & \text{if } C \leq 0.08 \text{ mg m}^{-3} \\ \frac{\sum_{i=3}^{5} W_i P_i + W_1 P_{1,n}}{C_w} & \text{if } C > 0.08 \text{ mg m}^{-3}. \end{cases} \tag{14}$$

https://doi.org/10.5194/egusphere-2026-4398
Preprint. Discussion started: 6 August 2026

and

$$F_p = \begin{cases} \frac{(-12.5C+1)W_3P_3}{C_w} + \frac{\sum_{i=6}^{7} W_iP_i}{C_w} & \text{if } C \leq 0.08\,\text{mg m}^{-3} \\ \frac{\sum_{i=6}^{7} W_iP_i}{C_w} & \text{if } C > 0.08\,\text{mg m}^{-3}. \end{cases} \quad (15)$$

Finally, for all methods, Chl-a of each size class (C_p, C_n and C_m) was calculated by multiplying the fractions by the total Chl-a (C).

2.4 Optical measurements of ocean colour on PICCOLO

2.4.1 Radiometric data

We used a dataset of remote sensing reflectance (R_{rs}) measurements collected during the PICCOLO cruise described by Sun et al. (2025a). These measurements were obtained using a Satlantic HyperSAS system consisting of one irradiance sensor (E_s) and two radiance sensors measuring sky radiance (L_i) and total sea-surface radiance (L_t). Raw radiometric measurements were dark-corrected, synchronised in time, and quality controlled following procedures in previous studies (Brewin et al., 2016; Lin et al., 2022). Quality control included filtering based on solar zenith angle, sensor viewing geometry, platform pitch and roll, and removal of records affected by sun glint or negative radiometric signals. R_{rs} was calculated as

$$R_{rs}(\lambda) = \frac{L_t(\lambda) - 0.028L_i(\lambda)}{E_s(\lambda)}, \quad (16)$$

with the value of 0.028 taken from Mobley (1999) and λ represents wavelength (nm). Additional near-infrared corrections were applied to reduce residual surface reflection effects as well as a correction for contamination of the E_s data from exhaust fumes on the ship (see Sun et al., 2025a; Heywood and Bell, 2024). Spectra with negative visible-band values or unstable spectral band ratios were removed. The remaining spectra were aggregated to 1-minute median values. For data at stations, the valid 1-minute median values were averaged within a $\pm$1 h time window according to the station definitions used during the cruise. Only R_{rs} ratio data were used in this paper for computing Chl-a, which was found to be insensitive to the correction for contamination of E_s data from exhaust fumes on the ship (see Heywood and Bell, 2024). Further details of the processing and quality control procedures are provided by Sun et al. (2025a).

2.4.2 Ocean colour Chl-*a* algorithms

Chl-a was estimated from the R_{rs} measurements using an commonly-used empirical, polynomial, band-ratio chlorophyll algorithm (O'Reilly et al., 2000), that relates the log-transformed ratio of blue to green remote-sensing reflectances (X) to Chl-a (C). X is first computed as

$$X = \log_{10}\{\max[R_{rs}(443), R_{rs}(490), R_{rs}(510)]/R_{rs}(555)\}. \quad (17)$$

Chl-a (C) is then estimated according to

$$C = 10^{(q_0+q_1X+q_2X^2+q_3X^3+q_4X^4)}, \quad (18)$$

https://doi.org/10.5194/egusphere-2026-4398
Preprint. Discussion started: 6 August 2026

where q_0, q_1, q_2, q_3 and q_4 are empirical coefficients. We used both a global set of coefficients following O'Reilly and Werdell (2019), where $q_0 = 0.32814$, $q_1 = -3.20725$, $q_2 = 3.22969$, $q_3 = -1.36769$ and $q_4 = -0.81739$, and a set of coefficients regionally-tuned to the Southern Ocean waters (∼25-160°E, not inclusive of the Weddell Sea) following Johnson et al. (2013), where $q_0 = 0.6736$, $q_1 = -2.0714$, $q_2 = -0.4939$, $q_3 = 0.4756$ and $q_4 = 0.0$. We also tested the algorithm of Ferreira et al. (2022) tuned to data primarily from the western Antarctic Peninsula. Similar to Eq. 18, the Ferreira et al. (2022) algorithm can be expressed as

$$C = 10^{Y(X)}, \tag{19}$$

but in this case, $Y(X)$ is expressed as

$$Y(X) = \begin{cases} A(X), & 10^X < 3, \\ (1-w)A(X) + wB(X), & 3 \le 10^X \le 5, \\ B(X), & 10^X > 5, \end{cases} \tag{20}$$

with

$$w = \frac{10^X - 3}{2}. \tag{21}$$

The terms $A(X)$ and $B(X)$ are expressed as

$$A(X) = 0.60159 - 3.20362X + 11.17268X^2 - 26.78898X^3 + 18.64112X^4, \tag{22}$$

and

$$B(X) = 0.63668 - 1.94561X + 0.15707X^2 - 0.57160X^3. \tag{23}$$

Essentially, $A(X)$ is applied when $10^X < 3$, $B(X)$ is applied when $10^X > 5$, and a linear interpolation between the two formulations is used for $3 \le 10^X \le 5$.

2.5 PICCOLO data compilation

The SFF, HPLC, and R_{rs} datasets were matched using the station definitions established during the PICCOLO cruise (within 24 h, typically no more than 1 km apart in distance). Because the vessel was occasionally in motion while occupying a station, underway R_{rs} measurements at some stations included multiple observations collected at slightly different geographic positions but within the same station period. These observations were therefore treated as belonging to a single station. When multiple R_{rs} measurements were available within a station, the observation closest to the SFF data in time was selected. For the HPLC dataset, measurements were matched to the corresponding SFF station, provided they were defined as the same station, even if they originated from different CTD casts conducted at different times. Depth matching was performed using the nearest available sampling depth. Additional details on the number of matched observations are provided in Table 1.

https://doi.org/10.5194/egusphere-2026-4398
Preprint. Discussion started: 6 August 2026

2.6 Statistical analysis

Three statistical tests were used to compare Chl-*a* and size-fractionated Chl-*a* derived using the HPLC-DPA and SFF, as well as to assess the agreement between R_{rs}-derived and in-situ Chl-*a*. These included the Pearson linear correlation coefficient (r), using the *scipy.stats.pearsonr* SciPy Python module, the centre-patterned (or unbiased) root mean square error (Δ, an index of precision) and the bias (δ, an index of accuracy). Δ and δ were calculated according to

$$\Delta = \left(\frac{1}{N} \sum_{i=1}^{N} \left\{ \left[X_{i,E} - \left(\frac{1}{N} \sum_{j=1}^{N} X_{j,E} \right) \right] - \left[X_{i,M} - \left(\frac{1}{N} \sum_{k=1}^{N} X_{k,M} \right) \right] \right\}^2 \right)^{1/2}, \tag{24}$$

and

$$\delta = \frac{1}{N} \sum_{i=1}^{N} \left(X_{i,E} - X_{i,M} \right), \tag{25}$$

where X is the variable (Chl-*a*) and N is the number of samples. The subscript E denotes the estimated variable and M the measured variable. For the comparison between HPLC-DPA and SFF, we assume that SFF is the measured and HPLC-DPA is the estimated, though, as stated in the introduction, both methods have uncertainties. All analyses were conducted in $\log_{10}$ space because Chl-*a* is generally well described by a log-normal distribution (Campbell, 1995). Accordingly, only observations for which both the HPLC- and SFF-derived size-fractionated Chl-*a* were not zero were included in the comparison.

2.7 Satellite data

Daily merged netCDF products of R_{rs} from the European Space Agency (ESA) Ocean Colour Climate Change Initiative (OC-CCI; version 6.0, 4 km resolution) were downloaded from the OC-CCI website (https://www.oceancolour.org) for the period spanning 18 January 2024 (the first station occupation) to 2 March 2024 (the final station occupation) (Sathyendranath et al., 2019). Data were extracted for the Weddell Sea sector of the Southern Ocean, bounded by 90 °W to 0 ° longitude and 85 °S to 50 °S latitude. Four R_{rs} bands (443, 490, 510, and 560 nm) were extracted from each daily file. Invalid and non-positive values were masked prior to further processing. Chl-*a* concentrations were estimated using the algorithm of Ferreira et al. (2022) (Eqs. 19–23), with the 560 nm band treated as equivalent to 555 nm. Chl-*a* was computed independently for each daily image, and a temporal median composite was then generated over the full study period (18 January to 2 March 2024). This composite Chl-*a* product was used as input to the three-component model (Eqs. 1–4) to map the fractional contributions of each phytoplankton size class of total Chl-*a* over the duration of the cruise. We also used the NOAA/NSIDC Climate Data Record of Passive Microwave Sea Ice Concentration dataset (Meier et al., 2024) of daily sea ice area fraction. Data were downloaded (http://nsidc.org/data/g02202/versions/6) for the same period as OC-CCI data (18 January to 2 March 2024) and averaged into a single composite to provide spatial context of sea ice dynamics during the PICCOLO cruise.

https://doi.org/10.5194/egusphere-2026-4398
Preprint. Discussion started: 6 August 2026

3 Results and discussion

3.1 Comparison of DPA and SFF estimates of size-fractionated Chl-*a* in the northwestern Weddell Sea

Coincident measurements of total Chl-*a* obtained using two independent methods (HPLC and SFF) showed good agreement during the PICCOLO cruise (Figure 1; $r = 0.914$, $\Delta = 0.157$), with low bias ($\delta = 0.013$). These results were similar to equivalent comparisons conducted on a much larger HPLC and SFF dataset compiled in tropical and subtropical waters (50°N to 50°S) during the AMT cruises (see Figure 2B of Brewin et al. (2014a); $r = 0.933$, $\Delta = 0.157$, $\delta = -0.024$, $N = 466$), as well as coincident fluorometric- and HPLC-derived Chl-*a* observations compiled from the globally representative NASA NOMAD dataset (see Figure 6 of Werdell and Bailey, 2005). Together, these results provide confidence in the Chl-*a* datasets collected during PICCOLO.

The four DPA methods successfully reconstructed Chl-*a* (C_w, see Eq. 5) from the seven diagnostic pigments (Figure 2a–d) with high correlation ($r > 0.97$) and good precision ($\Delta < 0.101$), in agreement with studies that have tested these methods in other regions (e.g., Brewin et al., 2015; Chase et al., 2020; Gittings et al., 2019, 2025; Sun et al., 2023). The correlation (r) was slightly higher, and the precision (Δ) slightly better, for the methods of Sun et al. (2023, 2025a). But the highest accuracy (δ closest to zero) was seen in the methods of Sun et al. (2023) and Chase et al. (2020). Statistical results from the comparison between DPA and SFF estimates of size-fractionated Chl-*a* (Figure 2e–h) are again similar to equivalent comparisons conducted in the Atlantic Ocean (see Table 2 and Figure 3 of Brewin et al. (2014a), and Figure 2 of Brewin et al. (2017a) for comparison), with Δ ranging from 0.155 to 0.513. However, performance varied among methods and size classes.

For microphytoplankton (Figure 2e–h), Δ was highest (i.e., precision lowest), ranging from 0.312 to 0.513, consistent with other comparisons (Brewin et al., 2014a, 2017a), but with generally good correlation over the Chl-*a* range ($r > 0.67$). All methods tended to overestimate Chl-*a* for microphytoplankton when compared with SFF ($\delta > 0.12$), with the Sun et al. (2025a) method having the lowest bias ($\delta = 0.126$) but the highest Δ (0.513). This overestimation could be related to the presence of small fucoxanthin-containing diatoms (e.g. *Nitzschia*, *Cylindrotheca*, and *Pseudo-nitzschia*) observed during the cruise (data not shown), although some methods are designed to account for and correct for this contribution. It is also worth noting that some nano-sized diatoms form chains, possess spines, or have elongated, thin morphologies, meaning they may be classified as microplankton based on filtration.

For nanophytoplankton (Figure 2i–l), the Chase et al. (2020) method outperformed the other three methods (which showed broadly similar statistics, and a tendancy to underestimate nanophytoplankton Chl-*a*), with the highest correlation, lowest Δ, and a δ closest to zero (Figure 2j). For picophytoplankton (Figure 2m–p), the opposite pattern was observed, with the Chase et al. (2020) method performing least well (Figure 2n). The Uitz et al. (2006) method showed the highest correlation for phytoplankton (Figure 2m), while the Sun et al. (2023) and Sun et al. (2025a) methods exhibited the lowest bias (δ).

Overall, the results suggest that the DPA method for estimating size-fractionated Chl-*a* compares as well with SFF data in the northwestern Weddell Sea as it does in the tropical and temperate waters of the Atlantic (Brewin et al., 2014a, 2017a). However, there are differences in individual methods across the three size classes (Figure 2). Methods were often systematically higher for

https://doi.org/10.5194/egusphere-2026-4398
Preprint. Discussion started: 6 August 2026

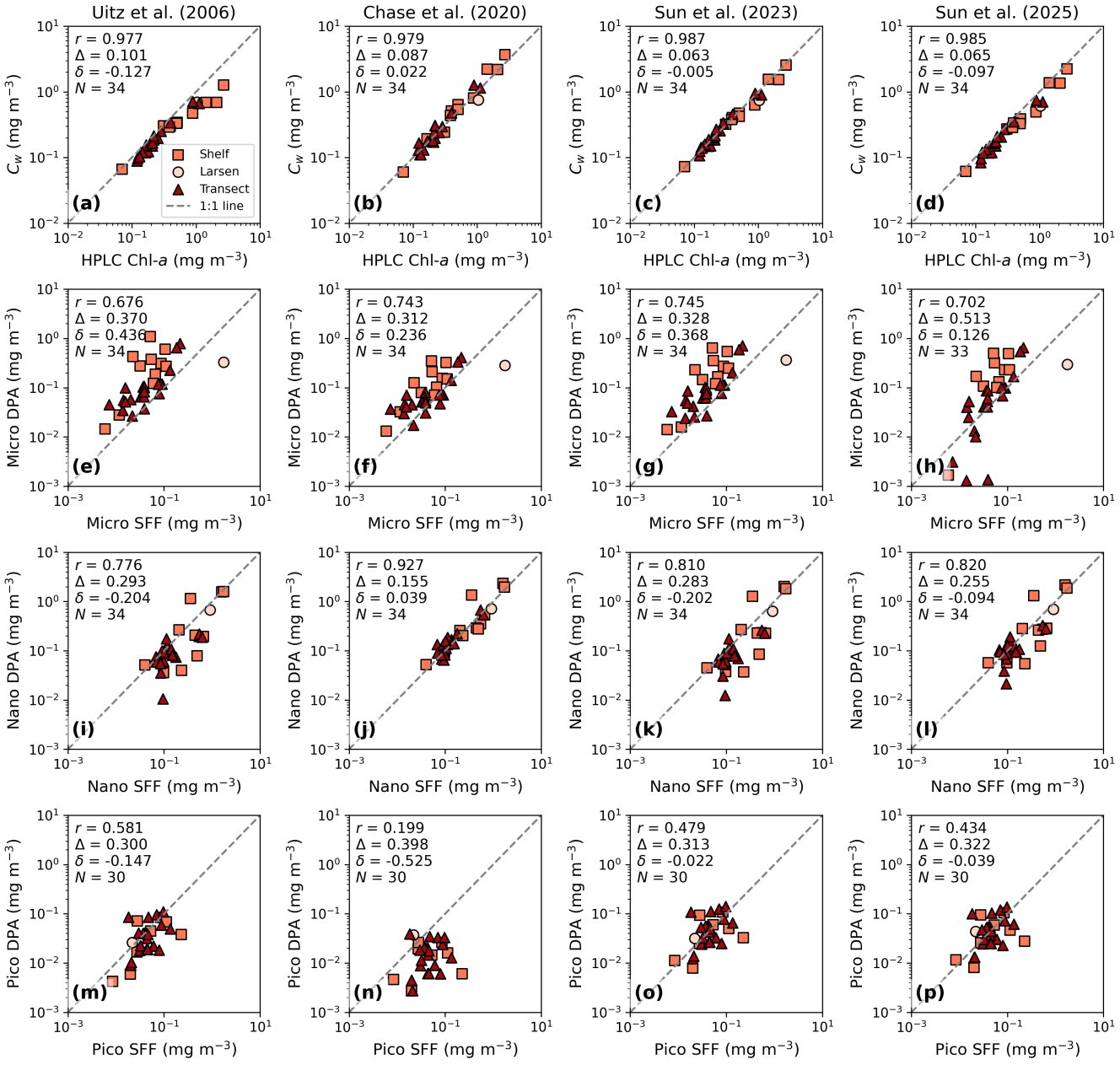

Figure 2. (a–d) Accuracy of DPA methods for reconstructing Chl-*a* from the seven diagnostic pigments (C_w) using the methods of (a) Uitz et al. (2006), (b) Chase et al. (2020), (c) Sun et al. (2023), and (d) Sun et al. (2025a). (e–p) Comparison of DPA and SFF estimates of size-fractionated Chl-*a* using the methods of (e, i and m) Uitz et al. (2006), (f, j, n) Chase et al. (2020), (g, k, o) Sun et al. (2023), and (h, l and p) Sun et al. (2025a), for (e–h) micro-, (i–l) nano- and (m–p) pico-phytoplankton Chl-*a*.

https://doi.org/10.5194/egusphere-2026-4398
Preprint. Discussion started: 6 August 2026

one size class (typically microphytoplankton) and consequently systematically lower for another (typically nanophytoplankton, but picophytoplankton in the case of Chase et al. (2020)).

3.2 Comparison of remote-sensing algorithms for Chl-*a* concentration in the northwestern Weddell Sea

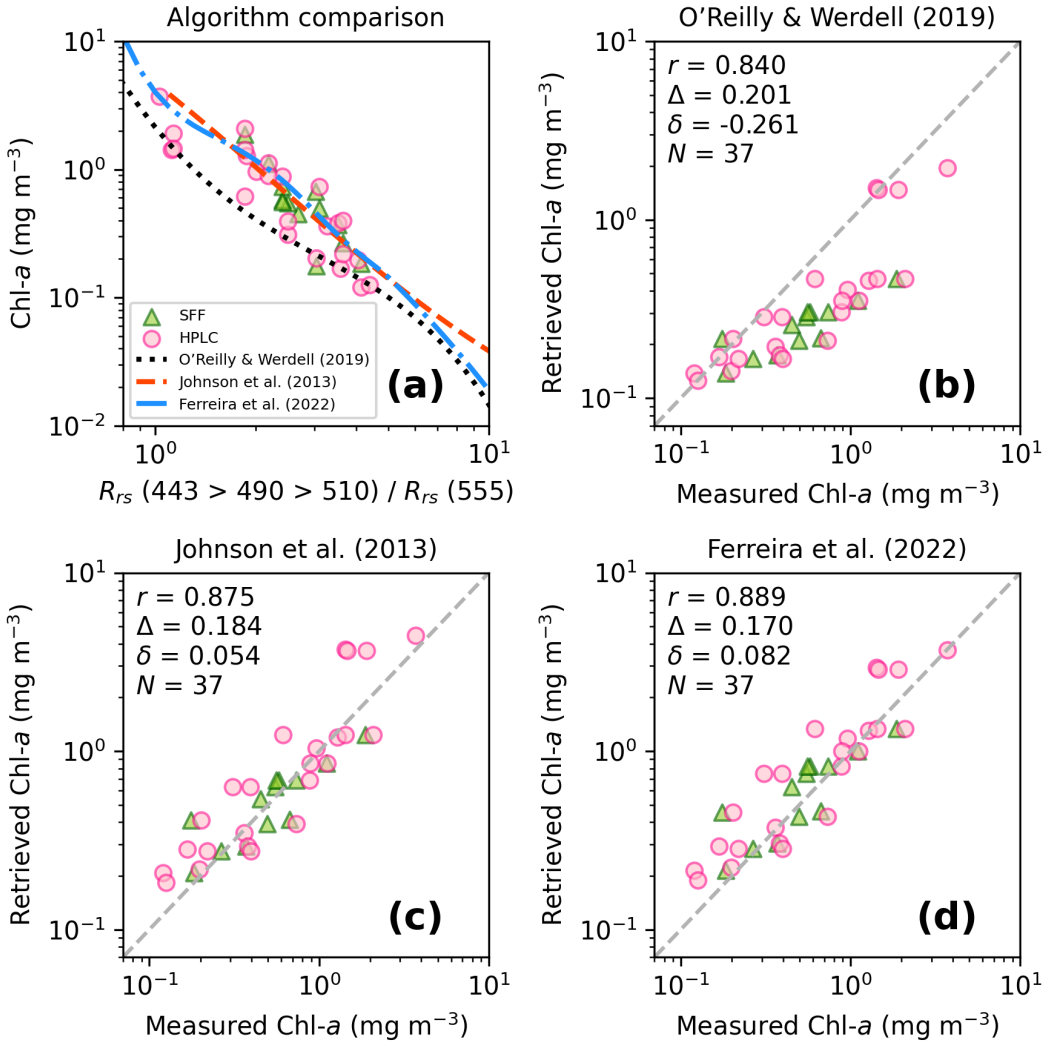

Figure 3. (a) Chl-*a* as a function of the maximum band ratio of remote sensing reflectance (R_{rs}), with PICCOLO *in-situ* data and algorithms overlain. (b–d) Scatter plots of retrieved Chl-*a* versus *in-situ* Chl-*a* for (b) the global algorithm of O'Reilly and Werdell (2019), (c) the Southern Ocean algorithm of Johnson et al. (2013), and (d) the western Antarctic Peninsular algorithm of Ferreira et al. (2022).

340 Coincident R_{rs} and total Chl-*a* data from PICCOLO revealed a clear inverse relationship between Chl-*a* and the maximum-band ratio ($R_{rs}(443 > 490 > 510)/R_{rs}(555)$), which is characteristic of the three empirical algorithms tested (Figure 3a). This

https://doi.org/10.5194/egusphere-2026-4398
Preprint. Discussion started: 6 August 2026

pattern is also evident in the validation plots, with all three algorithms showing high correlations between retrievals and in-situ Chl-*a* (Figure 3b–d; $r \geq 0.84$). The globally tuned algorithm of O'Reilly and Werdell (2019) systematically underestimated Chl-*a* when compared with in-situ measurements (Figure 3a–b). For a given Chl-*a*, the maximum-band ratio is consistently higher (i.e., waters appear optically bluer) in the PICCOLO dataset than in the global relationship of O'Reilly and Werdell (2019) (Figure 3a). Interestingly, Brewin and Dall'Olmo (2024) also reported that waters appeared bluer during the PICCOLO cruise than in tropical waters of similar transparency. This observed bio-optical anomaly is a characteristic feature of the Southern Ocean (but see Haëntjens et al., 2017, where the anomaly was not seen) and has been observed across several regions within it (Clementson et al., 2001; Garcia et al., 2005; Szeto et al., 2011). It has been linked to regional variations in the inherent optical properties of seawater (Mitchell, 1992; Dierssen and Smith, 2000; Reynolds et al., 2001; Ortega-Retuerta et al., 2010; Robinson et al., 2021; Li et al., 2024, 2026) which motivated the development of regional Chl-*a* algorithms (Johnson et al., 2013; Ferreira et al., 2022; Cha et al., 2025).

Both regional algorithms of Johnson et al. (2013) and Ferreira et al. (2022) compared well with the in-situ data (Figure 3a), with biases (δ) fairly close to zero (Figure 3c,d). The algorithm of Ferreira et al. (2022) showed marginally better correlation and precision (Δ), possibly because it was tuned in nearby waters (the western Antarctic Peninsula). The comparison between the Ferreira et al. (2022) model and in-situ data ($r = 0.889$, $\Delta = 0.170$, $\delta = 0.082$) is comparable (statistics only marginally lower) to the differences between HPLC and SFF estimates of Chl-*a* (Figure 1, $r = 0.914$, $\Delta = 0.157$, $\delta = 0.013$), highlighting the potential of using radiometric measurements to study phytoplankton dynamics in the region.

The underestimation of remotely-sensed Chl-*a* using a globally tuned algorithm (Figure 3a,b) in the northwestern Weddell Sea has also been reported by Salyuk et al. (2025). They attributed this bias to low chlorophyll-specific phytoplankton absorption (driven by high pigment packaging and the presence of large cells), low non-phytoplankton particle absorption, and low coloured dissolved organic matter absorption, relative to global ocean averages. The causes of optical anomalies in the seas surrounding Antarctica remains an active area of investigation (Sun et al., 2025a; Li et al., 2026).

3.3 Phytoplankton size structure in the northwestern Weddell Sea

Box plots of the fractional contributions of the three size classes to total Chl-*a* reveal a strong dominance of nanophytoplankton during the PICCOLO cruise, contributing around 60% of total Chl-*a* (Figure 4a). This is followed by microphytoplankton while picophytoplankton contribute the least. When broken down into the three regions (Transect (off-shelf), shelf, and Larsen), picophytoplankton contribute highest in the off-shelf (Transect) region ($\sim$20%; Figure 4e), where total Chl-*a* concentrations were lowest ($\sim$0.2 mg m^{-3}; Figure 4h). Their contribution decreases to $\sim$10% in shelf waters (Figure 4f), where total Chl-*a* concentrations are higher (Figure 4h), and falls to near zero in the highly productive Larsen shelf waters (Figure 4g,h). Nanophytoplankton show the greatest contribution on the shelf (Figure 4f), slightly lower off-shelf (Transect) with the lowest at Larsen (Figure 4e,g). In contrast, microphytoplankton dominate the high Chl-*a* waters of Larsen ($> 80\%$; Figure 4g,h), while exhibiting lower but similar contributions in both shelf and off-shelf (Transect) waters (Figure 4e,f).

The fractions of the three size classes at Rothera (Figure 4b) were broadly similar to PICCOLO (Figure 4a), but with a marginally higher (lower) contribution from microphytoplankton (nanophytoplankton) reflected in a higher total Chl-*a* (Figure

https://doi.org/10.5194/egusphere-2026-4398
Preprint. Discussion started: 6 August 2026

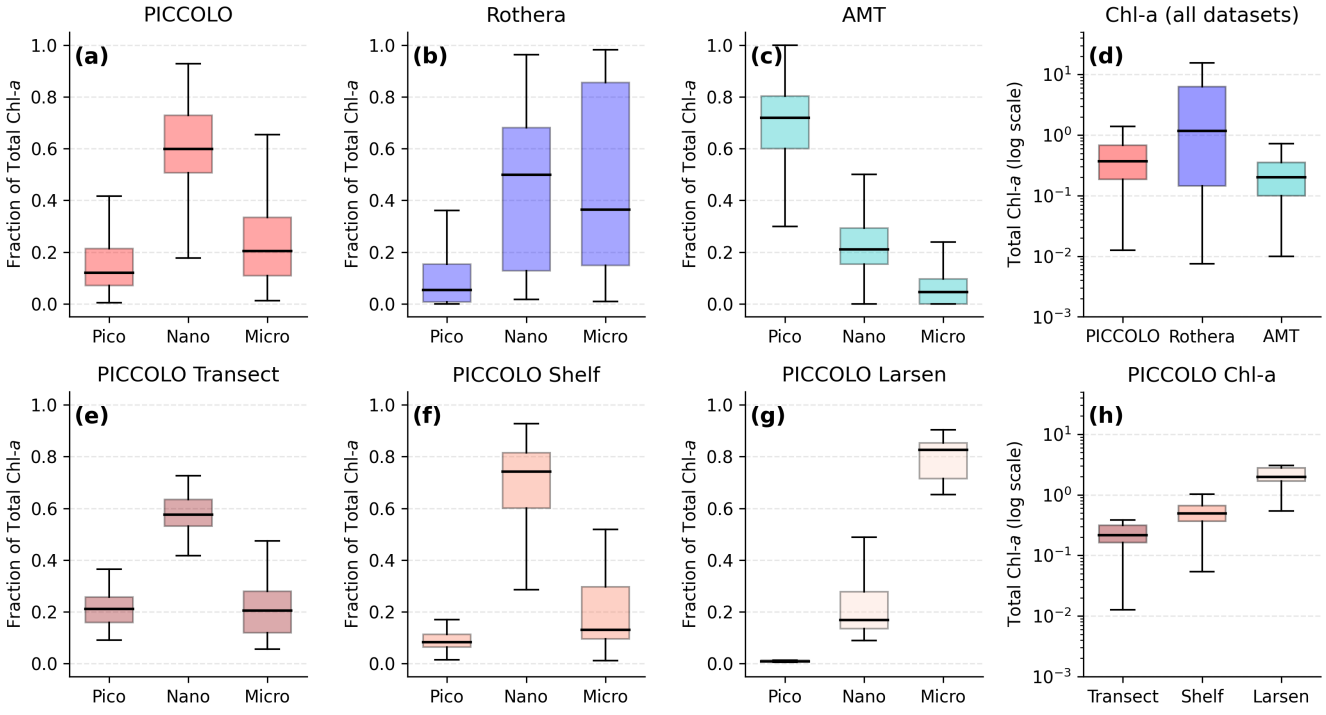

Figure 4. Box plots of the fractions of total Chl-*a* for pico-, nano- and micro-phytoplankton, for (a) PICCOLO, (b) Rothera and (c) AMT data, and PICCOLO data partitioned into (e) transect, (f) shelf and (g) Larsen. Plots (d) and (h) show box plots of the Chl-*a* for these datasets. The box spans the first to third quartiles, with the line inside indicating the median. The box height represents the interquartile range and the whiskers extend to the smallest and largest non-outlier values.

4d), and a much larger range of variability in these size classes, likely representing the broader seasonal conditions sampled at Rothera. Like PICCOLO, Rothera data indicate a very low contribution from picophytoplankton to total Chl-*a*. This is in stark contrast to the AMT data where picophytoplankton dominate total Chl-*a* (>70%), and nano- and microphytoplankton contributions are much lower (Figure 4c).

Table 2. Fitted parameters of the three-component model of Brewin et al. (2010) to PICCOLO, Rothera, and AMT SFF datasets. Uncertainties represent one standard deviation parameter uncertainties derived from the covariance matrix of the fits.

Model Parameter	PICCOLO	Rothera	AMT	Units
$C^m_{p,n}$	1.477 ± 0.291	1.30 ± 0.069	2.589 ± 0.186	mg m^{-3}
C^m_p	0.073 ± 0.010	0.098 ± 0.009	1.092 ± 0.089	mg m^{-3}
$D_{p,n}$	0.849 ± 0.029	0.844 ± 0.012	0.966 ± 0.007	dimensionless
D_p	0.288 ± 0.025	0.189 ± 0.005	0.747 ± 0.007	dimensionless

https://doi.org/10.5194/egusphere-2026-4398
Preprint. Discussion started: 6 August 2026

The Chl-*a* concentrations and the fractions of the three size classes are plotted as a function of total Chl-*a* for the three datasets (PICCOLO, Rothera, and AMT), with fits from the three-component model overlain (see parameters in Table 2; Figure 5a–f). In all three cases, the model captures the general shifts in size structure within the individual datasets as Chl-*a* increases. All three datasets show an increasing contribution of microphytoplankton with increasing total Chl-*a*, with the two Southern Ocean datasets (PICCOLO and Rothera) exhibiting slightly elevated microphytoplankton contributions ($\sim$17%) at lower total Chl-*a* compared with AMT (Figure 5g).

The main differences among the datasets emerge in the two smaller size classes. Across a much broader range of Chl-*a* (0.01–3 mg m^{-3}), the Antarctic datasets (PICCOLO and Rothera) show a substantially higher fraction of nanophytoplankton (Figure 5h) and a much lower fraction of picophytoplankton (Figure 5i) than on AMT. Although not all model parameters are statistically similar (Table 2), the model fits for the PICCOLO and Rothera datasets are closely aligned (Figure 5g–i), suggesting that the macroecological patterns in phytoplankton size structure are broadly similar across the western and eastern Antarctic Peninsula, and strikingly different from those in lower-latitude subtropical regions (AMT).

The low contribution of picophytoplankton to total Chl-*a* has also been observed in other regions of the Southern Ocean (Ward, 2015; Sun et al., 2023, 2025a). Flow cytometry data collected during PICCOLO (Tarran, 2026) indicate a complete absence of photosynthetic picocyanobacteria (*Prochlorococcus* and *Synechococcus*), which are known to dominate phytoplankton abundance and biomass in lower-latitude subtropical and temperate regions (Flombaum et al., 2013; Lange et al., 2018, 2020), with the picophytoplankton assemblages on PICCOLO primarily composed of picoeukaryotes.

Surface *in-situ* total Chl-*a* samples from PICCOLO are overlain on a satellite composite generated using the Ferreira et al. (2022) algorithm for the duration of the PICCOLO cruise (Figure 6a), and show broad agreement consistent with previous validation studies in the western Antarctic Peninsula and with summer satellite composites (Ferreira et al., 2022, 2024). Both datasets indicate lower concentrations offshore in the open waters of the Weddell Sea and higher concentrations on the shelf and near Larsen. The extensive sea-ice cover highlights the challenges associated with using ocean-colour data in this region.

Maps of the fractional contributions of the three size classes to total Chl-*a* (Figure 6b–d) were generated by forcing the three-component model (Eq. 1–4) with the satellite Chl-*a* data (Figure 6a) using parameters derived from the PICCOLO dataset (Table 2). The overlain surface *in-situ* fractions collected during PICCOLO are in broad agreement with the satellite estimates (acknowledging that they are not entirely independent). Microphytoplankton contributions are higher on the shelf and near Larsen (Figure 6b) and lower offshore, whereas picophytoplankton contributions are generally lower across the wider Weddell Sea and Antarctic Peninsula region, but increase slightly off-shelf and in the open waters of the Weddell Sea (Figure 6d). The satellite maps reveal a broad dominance of nanophytoplankton, contributing more than 60% of total Chl-*a* across most of the region (Figure 6c). There is some evidence that the satellite data underestimate nanophytoplankton (and overestimate microphytoplankton) on the shelf (Figure 6b–c). However, it is important to note that the temporal scales of the two datasets differ substantially, with the *in-situ* data representing instantaneous measurements and the satellite data representing averages over the duration of the cruise during clear-sky and ice-free conditions.

SFF measurements collected on PICCOLO are among the first, to our knowledge, obtained from the northwestern Weddell Sea shelf and the Larsen region. With the exception of very nearshore regions and bloom conditions (e.g., at Larsen), where

https://doi.org/10.5194/egusphere-2026-4398
Preprint. Discussion started: 6 August 2026

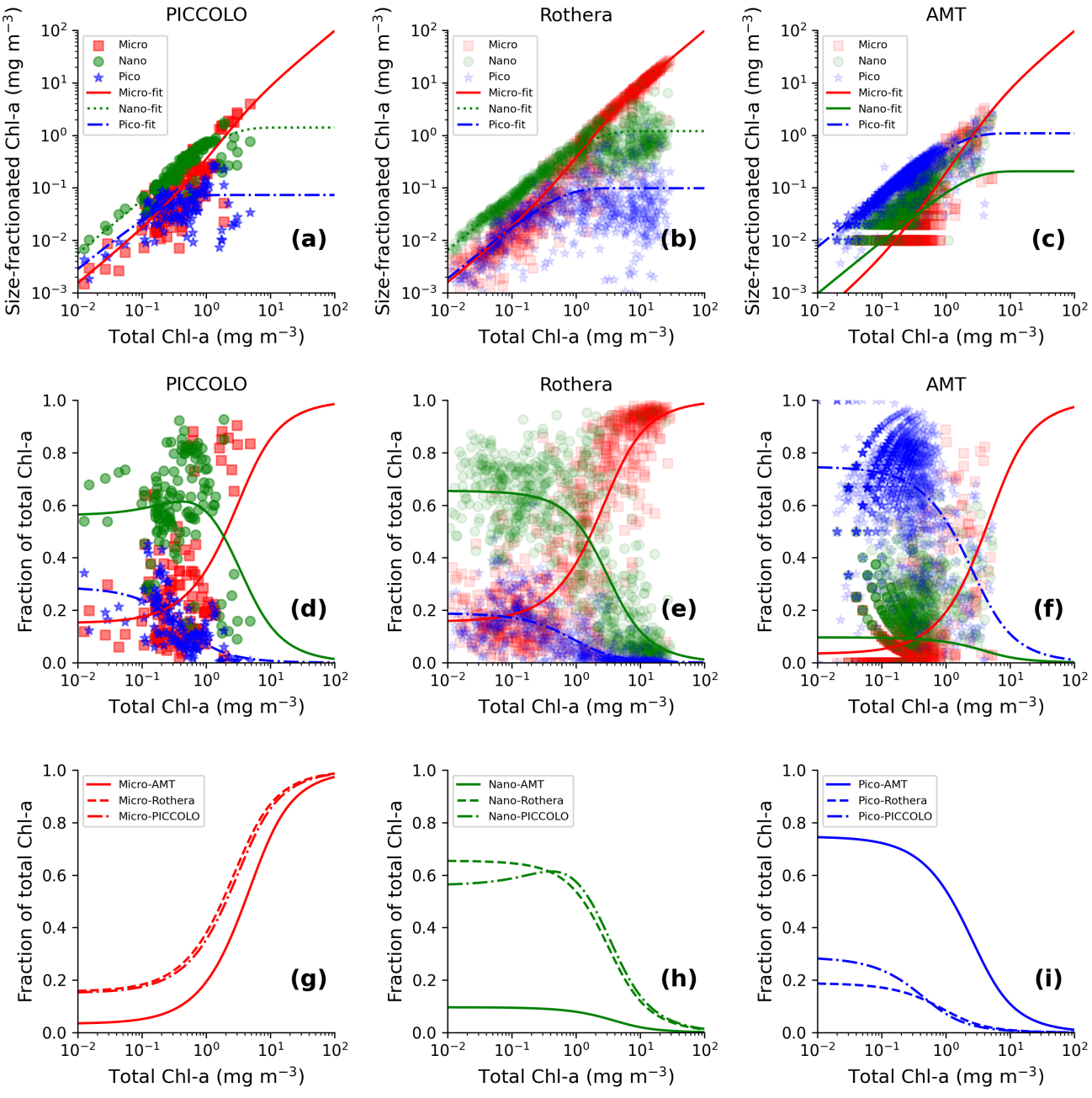

Figure 5. (a–c) pico-, nano-, and micro-phytoplankton chlorophyll concentrations and (d–e) the fractions of these size classes to total Chl-*a*, plotted as a function of total Chl-*a*, with the three-component model (parameters from Table 2), overlain, for (a,d) PICCOLO, (b, e) Rothera, and (c,f) AMT datasets. (g–i) model fits for (g) micro-, (h) nano-, and (i) pico-phytoplankton for the three datasets compared.

https://doi.org/10.5194/egusphere-2026-4398
Preprint. Discussion started: 6 August 2026

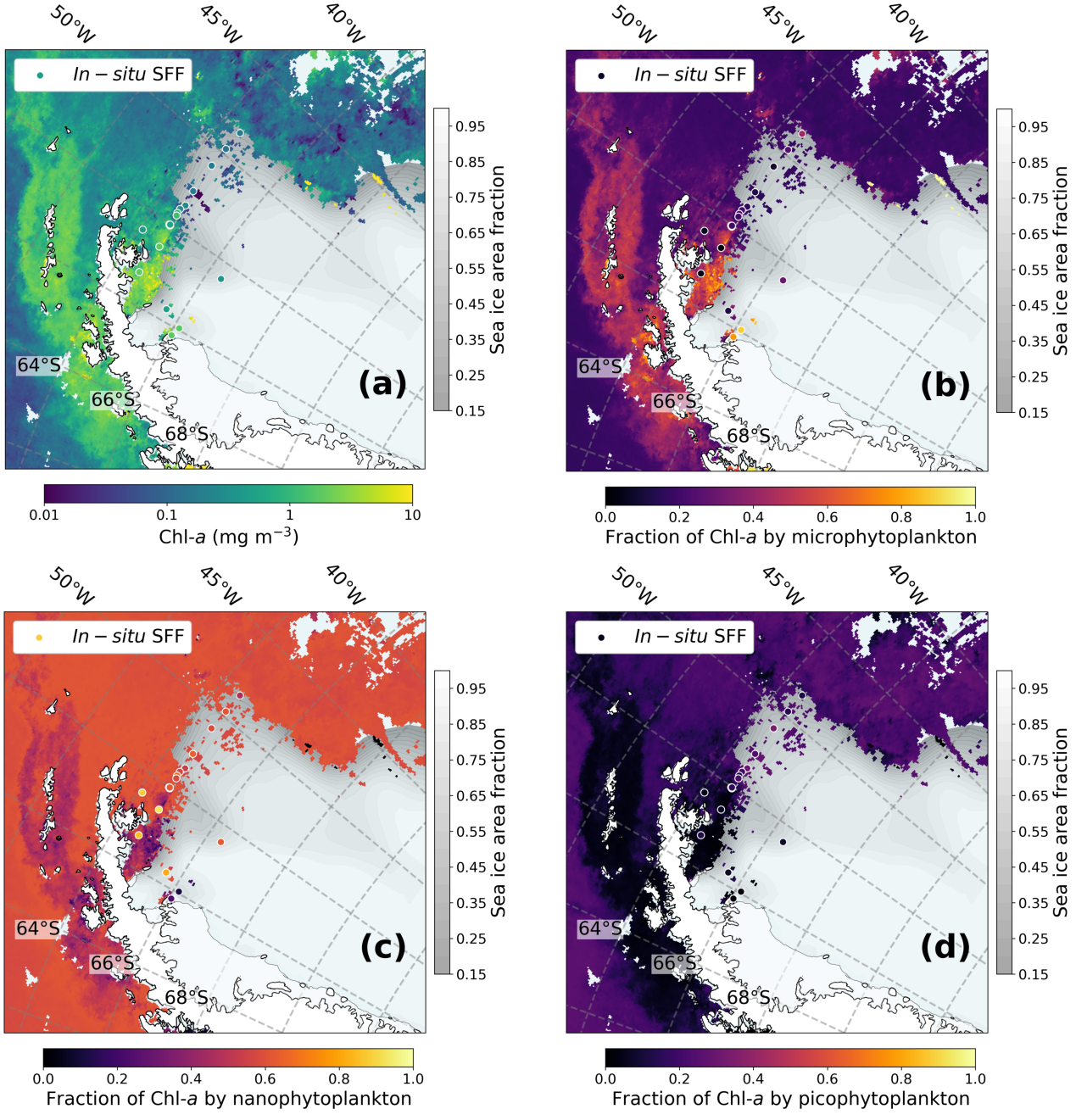

Figure 6. Satellite ocean colour (OC-CCI) and sea ice area fraction (NOAA/NSIDC) averages over the duration of the PICCOLO cruise (18 January 2024 to 2 March 2024) in the northwestern Weddell Sea. (a) Chl-*a* using the algorithm of Ferreira et al. (2022), (b–d) the fraction of Chl-*a* by micro-, nano- and picophytoplankton respectively, using Eqs. 1–4 (Brewin et al., 2010, 2015) and the PICCOLO parameters in Table 2. *In-situ* SFF data from PICCOLO are overlain in white circles filled using the same colour scale as that used with the satellite imagery. An ice shelf layer is overlain onto the map, taken from the Scientific Committee on Antarctic Research (https://www.add.scar.org/), to illustrate the position of the Larsen and George VI ice shelves.

https://doi.org/10.5194/egusphere-2026-4398
Preprint. Discussion started: 6 August 2026

microphytoplankton can dominate (Figure 5g, see also Clarke and Leakey, 1996), the PICCOLO datasets confirm a general dominance of nanophytoplankton, consistent with data collected on the western Antarctic Peninsula (Rothera, Figure 5b,e) and apparent over a much broader scale (Figure 6c). This central role of nanophytoplankton has also been reported in the eastern Weddell Sea (Dower et al., 1996; Flynn et al., 2023), Drake Passage and the Indian sector of the Southern Ocean (Weber and El-Sayed, 1987), around the South Shetland Islands (Hewes, 2009; García-Muñoz et al., 2014), in the marginal ice zone of the northern Weddell Sea (Becquevort et al., 1992; Lancelot et al., 1993), and more broadly accross the Southern Ocean (Robinson et al., 2021). Nanoplankton-sized diatoms (e.g. *Chaetoceros spp.*) and nano-sized autotrophic flagellates (*Cryptomonas sp.*) have frequently been observed in and around the Weddell Sea (Becquevort et al., 1992; Mura et al., 1995; Mendes et al., 2023; Flynn et al., 2023).

Differences in resource supply (e.g. light and nutrients) are considered key drivers of biogeographic patterns in phytoplankton size structure (Marañón, 2015), though temperature and grazing play a role (Goericke, 2002; López-Urrutia and Morán, 2015). In oligotrophic regions (represented here by the AMT data), pico-sized phytoplankton can outcompete larger size classes due to their high surface-area-to-volume ratio and rapid nutrient diffusion across the boundary layer (Ward, 2024). Additional advantages of small cell size include efficient light absorption, reduced self-shading, and slow sinking rates (Chisholm, 1992). However, pico-sized cells generally have lower maximum growth rates because their limited internal space constrains the number of catalysts involved in biomass synthesis (Marañón et al., 2013). Under nutrient-replete conditions, nanophytoplankton are therefore expected to dominate, as they achieve high maximum growth rates by balancing sufficient intracellular space for catalysts with relatively short diffusion distances for efficient resource acquisition and biomass production (Marañón et al., 2013). In the medium-to-large size range, maximum growth rates decline again as nutrient assimilation is constrained by longer intracellular transport distances, reduced light absorption, and increased self-shading (Marañón et al., 2013). However, larger cells gain a major ecological advantage through reduced grazing pressure, due to the lower abundance and longer generation times of their metazoan grazers (Chisholm, 1992). In contrast, pico- and nanoplankton are often consumed by similarly sized mixotrophic or heterotrophic protists with short generation times. This trade-off helps explain why microphytoplankton blooms occur in the Southern Ocean, for example at the Larsen ice shelf (this study), on the highly productive South Georgia shelf (Korb et al., 2008), and during spring and autumn in the Scotia Sea (Korb et al., 2012). Interestingly, these microphytoplankton communities may primarily consist of colonies formed by nano-sized individual cells, combining the metabolic advantages of intermediate cell size with the grazing deterrence associated with larger size (e.g. chain-forming diatoms and *Phaeocystis spp.* colonies).

3.4 Limitations and recommendations

Although the PICCOLO measurements constitute a rare dataset on phytoplankton size structure, they were collected during a specific period of the year (late summer) and may therefore not be representative of other seasons. It is recommended that, should opportunities and platforms be available, similar measurements be collected at other times of the year (e.g., Viljoen et al., 2025), though we recognise that sea ice dynamics may make this challenging. Nonetheless, it is reassuring that the

https://doi.org/10.5194/egusphere-2026-4398
Preprint. Discussion started: 6 August 2026

macroecological patterns in size structure observed in PICCOLO agree well with data collected at Rothera (Figure 5), which is more representative of the full seasonal cycle, although collected on the opposite side of the peninsula.

Although the methodological protocols used at Rothera and during PICCOLO differ in their execution, both are designed to minimise the influence of phaeopigments on Chl-*a* estimates. Phaeopigment concentrations can be significant in the Southern Ocean, with implications for particle absorption and the accurate measurement of Chl-*a* (Robinson et al., 2021). The presence of diatoms containing chlorophyll-*c* pigments can also result in positive biases in fluorometrically derived Chl-*a*, due to overlap between the chlorophyll-*a* and chlorophyll-*c* emission spectra (Moutier et al., 2019). These issues are not thought to be important for PICCOLO, as comparisons with HPLC-derived Chl-*a* broadly indicate no systematic differences (Figure 1). However, they may have a greater impact at other times of the season, in specific locations of the Weddell Sea, and in other regions.

Although broad agreement was observed between SSF- and DPA-derived size-fractionated Chl-*a*, consistent with studies from lower-latitude regions (Brewin et al., 2014a), differences were apparent depending on the method used and the size class considered (Figure 2). Both methods are associated with uncertainties (as discussed in the Introduction) yet have been widely used for decades. New approaches for deriving size-fractionated Chl-*a* should therefore be explored further, such as automated quantitative cell imaging combined with conventional flow cytometry (Chase et al., 2020), and in-line underway size-fractionated spectrophotometry (Organelli et al., 2018).

Notwithstanding the importance of phytoplankton size as a master trait (Marañón, 2015), influencing both biogeochemistry and ecology, size is not always the most useful means of classifying phytoplankton for specific biogeochemical functions (IOCCG, 2014). For example, dimethyl sulfide (DMS)-producing phytoplankton occur within the nano-size class (e.g. *Phaeocystis*), alongside many other phytoplankton species that do not produce DMS. For certain biogeochemical applications, a taxonomic approach to phytoplankton classification may be more appropriate (Meyer et al., 2026a).

3.5 Implication for organic carbon cycling

Relative to lower-latitude regions, where picophytoplankton contribute substantially to the Chl-*a* standing stock, the northwestern Weddell Sea shelf and the broader region are dominated by nanophytoplankton (Figure 6). This may have important implications for the regional carbon cycle. For example, with knowledge of the photosynthetic efficiency of these phytoplankton size classes (e.g., Uitz et al., 2008), regional maps of size-fractionated Chl-*a* (e.g. Figure 6) could be combined with light models to quantify carbon production by these size classes at synoptic scales (e.g., Uitz et al., 2008; Brewin et al., 2017b; Curran et al., 2018), potentially improving estimates of carbon export (e.g. Siegel et al., 2014). This shift towards larger phytoplankton sizes may also propagate into changes in the slope of the plankton size spectrum, with implications for energy transfer efficiency through the food web (Sheldon et al., 1972; Platt and Denman, 1978; Atkinson et al., 2024). For example, picoplankton are generally too small for efficient ingestion by copepods, the dominant metazoan grazers, and are at the lower size limit for krill, whereas salps can consume them more effectively (Schmidt and Atkinson, 2016). Therefore, a shift from pico- to nanoplankton dominance may provide a more efficient pathway for energy transfer from primary producers to metazoans by reducing the number of trophic steps. This shift may be reflected in a less steeply negative slope of the normalised biomass size spectrum, with implications for more efficient energy transfer through the food web.

https://doi.org/10.5194/egusphere-2026-4398
Preprint. Discussion started: 6 August 2026

Extreme and abrupt climate-driven changes in Antarctica are becoming more frequent (Wille et al., 2024), with implications for the iconic ecosystems that thrive in this extreme environment (Abram et al., 2025; Atkinson et al., 2025; Krumhardt et al., 2026) and for the biogeochemical cycles that sustain the planet (Boyd et al., 2024). Developing a better understanding of how phytoplankton dynamics are changing in regions such as the northwestern Antarctic continental shelf, where the processes controlling organic carbon cycling remain poorly constrained, is a research priority for predicting and mitigating the consequences of climate-driven change.

4 Conclusions

A dataset consisting of discrete measurements of size-fractionated Chl-*a*, obtained using *in-vitro* fluorescence size-fractionated filtration (SFF), HPLC pigments, and *in-situ* radiometric observations, collected in late summer 2024 in the northwestern Weddell Sea, was used to study phytoplankton size structure and Chl-*a* in this remote and rarely sampled region. These measurements were compared alongside a time series of SFF data collected at Rothera on the western Antarctic Peninsula, and from the AMT cruises in lower latitude regions (Figure 1). The following conclusions and recommendations were drawn:

- Estimates of size-fractionated Chl-*a* derived from diagnostic pigment analysis (DPA) of HPLC data are in broad agreement with those obtained using SFF in this region, consistent with similar studies in lower latitude regions (Brewin et al., 2014a, 2017a). However, differences between individual methods were observed, along with some systematic biases across the three size classes. We recommend that new approaches for deriving size-fractionated Chl-*a* be tested alongside coincident DPA and SFF data, with the aim of improving the accuracy of *in-situ* size-fractionated Chl-*a* estimates while allowing consistency in long-term data series.

- We recommend the use of regionally tuned ocean-colour Chl-*a* algorithms in the northwestern Weddell Sea (e.g., Johnson et al., 2013; Ferreira et al., 2022), which were found to perform better than globally tuned algorithms that systematically underestimate Chl-*a*.

- Medium-celled phytoplankton (nanophytoplankton) dominate Chl-*a* in most of the northwestern Weddell Sea. This pattern is consistent with data collected at Rothera on the western Antarctic Peninsula, but contrasts strongly with lower latitude regions, where picophytoplankton tend to dominate. We recommend conducting similar measurements in the northwestern Weddell Sea at other stages of the seasonal cycle (e.g. spring), to determine whether different patterns emerge at other times of year.

- Macroecological size-structure patterns observed in the northwestern Weddell Sea are consistent with those in other ocean regions, with the fraction of microphytoplankton increasing with total Chl-*a*, and smaller phytoplankton (nano- and picophytoplankton) decreasing. However, the parameters of these relationships differ in both the northwestern Weddell Sea and the western Antarctic Peninsula, reflecting the dominance of nanophytoplankton at lower Chl-*a*, in contrast to picophytoplankton dominance at lower latitudes. Combining these relationships with satellite data could provide insights into organic carbon production at larger spatial scales.

https://doi.org/10.5194/egusphere-2026-4398
Preprint. Discussion started: 6 August 2026

Code availability. Code for processing the data is openly available on GitHub (https://github.com/rjbrewin/PICCOLO_Weddell_Sea_Phytoplankton_Size).

Data availability. The PICCOLO SFF data, HPLC and radiometric data are openly available through the British Oceanographic Data Centre (BODC Meyer et al., 2026b; Wilkinson, 2026). Rothera data are openly available through the UK Polar Data Centre (Clarke et al., 2022) AMT cruise data are openly available through the BODC. Satellite data used are openly available through the Ocean Colour Climate Change Initiative (http://www.oceancolour.org) and the National Snow and Ice Data Center (http://nsidc.org/data/g02202/versions/6).

Author contributions. RJWB drafted the manuscript. RJWB and XS performed the analysis. BW collected the SFF data, with support from SB, AR, IB and TB. RJWB, XS, GD, EC, MM and KH collected and facilitated the processing the HPLC data. RJWB, XS, GD, GT collected the radiometric data. AA, KS, QZ and JJV supported discussions on the manuscript. All authors contributed to and approved the final draft.

Competing interests. One of the co-authors is a member of the editorial board of Ocean Science. All other authors have no conflict of interest.

Acknowledgements. We sincerely thank the captain, crew, all the researchers, technicians, and data managers involved with cruise SD035 on the *RRS* Sir David Attenborough. We also thank all those involved in the collection of SFF data at Rothera and on AMT cruises. This work is part of the PICCOLO (Processes Influencing Carbon Cycling: Observations of the Lower limb of the Antarctic Overturning) project. PICCOLO is funded by the Natural Environment Research Council (NERC) grant numbers: NE/P021395/1 and NE/P021409/1. RB and XS were also supported by a UKRI FLF grant (MR/V022792/1). XS was also supported by the Collaborative Antarctic Science Scheme (CASS, British Antarctic Survey, 2023/24 season). RB, AA and JJV were also supported by a European Space Agency (ESA) project "Tipping points and abrupt changes In the Marine Ecosystem (TIME)". EC was also supported by the European Commission Directorate General for Defence Industry and Space (DG DEFIS) and the Copernicus Programme. During the preparation of this manuscript the authors used AI tools for the purpose of checking grammar, debugging code and for proofreading. We thank Andy Rees for supporting the work.

https://doi.org/10.5194/egusphere-2026-4398
Preprint. Discussion started: 6 August 2026

References

Abram, N. J., Purich, A., England, M. H., McCormack, F. S., Strugnell, J. M., Bergstrom, D. M., Vance, T. R., St, T., Wienecke, B., Heil, P., Doddridge, E. W., Sallée, J.-B., Williams, T. J., Reading, A. M., Mackintosh, A., Reese, R., Winkelmann, R., Klose, A. K., Boyd, P. W., Chown, S. L., and Robinson, S. A.: Emerging evidence of abrupt changes in the Antarctic environment, Nature, 644, 621–633, https://doi.org/10.1038/s41586-025-09349-5, 2025.

Atkinson, A., Hill, S. L., Reiss, C. S., Pakhomov, E. A., Beaugrand, G., Tarling, G. A., Yang, G., Steinberg, D. K., Schmidt, K., Edwards, M., Rombolá, E., and Perry, F. A.: Stepping stones towards Antarctica: Switch to southern spawning grounds explains an abrupt range shift in krill, Global Change Biology, 28, 1359–1375, https://doi.org/10.1111/gcb.16009, 2022.

Atkinson, A., Rossberg, A. G., Gaedke, U., Sprules, G., Heneghan, R. F., Batziakas, S., Grigoratou, M., Fileman, E., Schmidt, K., and Frangoulis, C.: Steeper size spectra with decreasing phytoplankton biomass indicate strong trophic amplification and future fish declines, Nature Communications, 15, 381, https://doi.org/10.1038/s41467-023-44406-5, 2024.

Atkinson, A., Pakhomov, E., Laurenson, A., Sullivan, E., Brewin, R. J. W., Holmes, C., Clewley, D., Schmidt, K., and Martinez-Vicente, V.: Implications of the recent loss of Antarctic sea ice for phytoplankton and summer feeding habitats of salps and krill, Marine Ecology Progress Series, 774, 1–16, https://doi.org/10.3354/meps15002, 2025.

Aumont, O., Maier-Reimer, E., Blain, S., and Monfray, P.: An ecosystem model of the global ocean including Fe, Si, P colimitations, Global Biogeochemical Cycles, 17, 1060, https://doi.org/10.1029/2001GB001745, 2003.

Becquevort, S., Mathot, S., and Lancelot, C.: Interactions in the microbial community of the marginal ice zone of the northwestern Weddell Sea through size distribution analysis, Polar Biology, 12, 211–218, https://doi.org/10.1007/BF00238262, 1992.

Biggs, T. E. G., Alvarez-Fernandez, S., Evans, C., Mojica, K. D. A., R., P. D., Venables, H. J., Pond, D. W., and Brussaard, C. P. D.: Antarctic phytoplankton community composition and size structure: Importance of ice type and temperature as regulatory factors, Polar Biology, 42, 1197–1215, https://doi.org/10.1007/s00300-019-02576-3, 2019.

Boyd, P. W., Arrigo, K. R., Ardyna, M., Halfter, S., Huckstadt, L., Kuhn, A. M., Lannuzel, D., Neukermans, G., Novaglio, C., Shadwick, E. H., Swart, S., and Thomalla, S. J.: The role of biota in the Southern Ocean carbon cycle, Nature Reviews Earth & Environment, 5, 390–408, https://doi.org/10.1038/s43017-024-00531-3, 2024.

Brewin, R. J. W. and Dall'Olmo, G.: Ocean-colour anomalies quantified by the human eye, Journal of Plankton Research, 46, 380–382, https://doi.org/10.1093/plankt/fbae027, 2024.

Brewin, R. J. W., Sathyendranath, S., Hirata, T., Lavender, S. J., Barciela, R., and Hardman-Mountford, N. J.: A three-component model of phytoplankton size class for the Atlantic Ocean, Ecological Modelling, 221, 1472–1483, https://doi.org/10.1016/j.ecolmodel.2010.02.014, 2010.

Brewin, R. J. W., Hirata, T., Hardman-Mountford, N. J., Lavender, S., Sathyendranath, S., and Barlow, R.: The influence of the Indian Ocean Dipole on interannual variations in phytoplankton size structure as revealed by Earth Observation, Deep Sea Research II, 77-80, 117–127, https://doi.org/10.1016/j.dsr2.2012.04.009, 2012.

Brewin, R. J. W., Sathyendranath, S., Lange, P. K., and Tilstone, G.: Comparison of two methods to derive the size-structure of natural populations of phytoplankton, Deep Sea Research I, 85, 72–79, https://doi.org/10.1016/j.dsr.2013.11.007, 2014a.

Brewin, R. J. W., Sathyendranath, S., Tilstone, G., Lange, P. K., and Platt, T.: A multicomponent model of phytoplankton size structure, Journal of Geophysical Research, 119, 3478–3496, https://doi.org/10.1002/2014JC009859, 2014b.

https://doi.org/10.5194/egusphere-2026-4398
Preprint. Discussion started: 6 August 2026

Brewin, R. J. W., Sathyendranath, S., Jackson, T., Barlow, R., Brotas, V., Airs, R., and Lamont, T.: Influence of light in the mixed layer on the parameters of a three-component model of phytoplankton size structure, Remote Sensing of Environment, 168, 437–450, https://doi.org/10.1016/j.rse.2015.07.004, 2015.

Brewin, R. J. W., Dall'Olmo, G., Pardo, S., van Dongen-Vogel, V., and Boss, E. S.: Underway spectrophotometry along the Atlantic Meridional Transect reveals high performance in satellite chlorophyll retrievals, Remote Sensing of Environment, 183, 82–97, https://doi.org/10.1016/j.rse.2016.05.005, 2016.

Brewin, R. J. W., Ciavatta, S., Sathyendranath, S., Jackson, T., Tilstone, G., Curran, K., Airs, R. L., Cummings, D., Brotas, V., Organelli, E., Dall'Olmo, G., and Raitsos, D. E.: Uncertainty in Ocean-Color Estimates of Chlorophyll for Phytoplankton Groups0, Frontiers in Marine Science, 4, 104, https://doi.org/10.3389/fmars.2017.00104, 2017a.

Brewin, R. J. W., Tilstone, G., Jackson, T., Cain, T., Miller, P., Lange, P. K., Misra, A., and Airs, R.: Modelling size-fractionated primary production in the Atlantic Ocean from remote sensing, Progress in Oceanography, 158, 130–149, https://doi.org/10.1016/j.pocean.2017.02.002, 2017b.

Brewin, R. J. W., Ciavatta, S., Sathyendranath, S., Skákala, J., Bruggeman, J., Ford, D., and Platt, T.: The Influence of Temperature and Community Structure on Light Absorption by Phytoplankton in the North Atlantic, Sensors, 19, 4182, https://doi.org/10.3390/s19194182, 2019a.

Brewin, R. J. W., Morán, X. A. G., Raitsos, D. E., Gittings, J. A., Calleja, M. L. l., Viegas, M., Ansari, M. I., Al-Otaibi, N., Huete-Stauffer, T. M., and Hoteit, I.: Factors Regulating the Relationship Between Total and Size-Fractionated Chlorophyll-*a* in Coastal Waters of the Red Sea, Frontiers in Microbiology, 10, 1964, https://doi.org/10.3389/fmicb.2019.01964, 2019b.

Brewin, R. J. W., Sathyendranath, S., Platt, T., Bouman, H., Ciavatta, S., Dall'Olmo, G., Dingle, J., Groom, S., Jönsson, B., Kostadinov, T. S., Kulk, G., Laine, M., Martínez-Vicente, M., Psarra, S., Raitsos, D. E., Richardson, K., Marie-Hélène, R., Rousseaux, C. S., Salisbury, J., Shutler, J. D., and Walker, P.: Sensing the ocean biological carbon pump from space: A review of capabilities, concepts, research gaps and future developments, Earth-Science Reviews, 217, 103 604, https://doi.org/10.1016/j.earscirev.2021.103604, 2021.

Brito, A. C., Sà, C., Brotas, V., Brewin, R. J. W., Silva, T., Vitorino, J., Platt, T., and Sathyendranath, S.: Effect of phytoplankton size classes on bio-optical properties of phytoplankton in the Western Iberian coast: Application of models, Remote Sensing of Environment, 156, 537–550, https://doi.org/10.1016/j.rse.2014.10.020, 2015.

Brotas, V., Brewin, R. J. W., Sá, C., Brito, A. C., Silva, A., Mendes, C. R., Diniz, T., Kaufmann, M., Tarran, G., Groom, S. B., Platt, T., and Sathyendranath, S.: Deriving phytoplankton size classes from satellite data: Validation along a trophic gradient in the eastern Atlantic Ocean, Remote Sensing Environment, 134, 66–77, https://doi.org/10.1016/j.rse.2013.02.013, 2013.

Butenschön, M., Clark, J., Aldridge, J. N., Allen, J. I., Artioli, Y., Blackford, J., Bruggeman, J., Cazenave, P., Ciavatta, S., Kay, S., Lessin, G., van Leeuwen, S., van der Molen, J., de Mora, L., Polimene, L., Sailley, S., Stephens, N., , and Torres, R.: ERSEM 15.06: a generic model for marine biogeochemistry and the ecosystem dynamics of the lower trophic levels, Geoscience Model Development, 9, 1293–1339, https://doi.org/10.5194/gmd-9-1293-2016, 2016.

Campbell, J. W.: The lognormal distribution as a model for bio-optical variability in the sea, Journal of Geophysical Research, 100(C7), 13 237–13 254, https://doi.org/10.1029/95JC00458, 1995.

Canuti, E.: Phytoplankton pigment in situ measurements uncertainty evaluation: an HPLC interlaboratory comparison with a European-scale dataset, Frontiers in Marine Science, 10, 1197 311, https://doi.org/10.3389/fmars.2023.1197311, 2023.

Cha, M., Pang, X., and Antoine, D.: Development of parameter-tuned algorithms for Chlorophyll-a concentration estimates in the Southern Ocean, Remote Sensing, 17, 3595, https://doi.org/10.3390/rs17213595, 2025.

https://doi.org/10.5194/egusphere-2026-4398
Preprint. Discussion started: 6 August 2026

Chase, A. P., Kramer, S. J., Haëntjens, N., Boss, E. S., Karp-Boss, L., Edmondson, M., and Graff, J. R.: Evaluation of diagnostic pigments to estimate phytoplankton size classes, Limnology and Oceanography: Methods, 18, 570–584, https://doi.org/10.1002/lom3.10385, 2020.

Chisholm, S. W.: Phytoplankton Size, in: Primary Productivity and Biogeochemical Cycles in the Sea, edited by Falkowski, P. G. and Woodhead, A. D., pp. 213–237, Springer, New York, 1992.

Clarke, A. and Leakey, R. J. G.: The seasonal cycle of phytoplankton, macronutrients, and the microbial community in a nearshore Antarctic marine ecosystem, Limnology and Oceanography, 41, 1281–1294, https://doi.org/10.4319/lo.1996.41.6.1281, 1996.

Clarke, A., Meredith, M., Venables, H., Hendry, K., Peat, H., ten Hoopen, P., Brandon, M., Henley, S., Annett, A., Leng, M., Arrowsmith, C., Chapman, A., Beaumont, J., Piper, R., Miller, A., Mann, P., Rossetti, H., Massey, A., Souster, T., and Clement, A.: Quasi-weekly, year-round oceanographic and ice measurements at the coastal Western Antarctic Peninsula from 1997 to 2018 (Version 1.0), https://doi.org/10.5285/50acb5b7-5b42-44cd-a98e-790bd367f204, 2022.

Claustre, H.: The Trophic Status of Various Oceanic Provinces as Revealed by Phytoplankton Pigment Signatures, Limnology and Oceanography, 39, 1206–1210, https://doi.org/10.4319/lo.1994.39.5.1206, 1994.

Clementson, L. A., Parslow, J. S., Turnbull, A. R., McKenzie, D. C., and Rathbone, C. E.: Optical properties of waters in the Australasian sector of the Southern Ocean, Journal of Geophysical Research: Oceans, 106, 31 611–31 625, https://doi.org/https://doi.org/10.1029/2000JC000359, 2001.

Corredor-Acosta, A., Morales, C. E., Brewin, R. J. W., Auger, P.-A., Pizarro, O., Hormazabal, S., and Anabalón, V.: Phytoplankton Size Structure in Association with Mesoscale Eddies off Central-Southern Chile: The Satellite Application of a Phytoplankton Size-Class Model, Remote Sensing, 10, 834, https://doi.org/10.3390/rs10060834, 2018.

Curran, K., Brewin, R. J. W., Tilstone, G. H., Bouman, H. A., and Hickman, A.: Estimation of Size-Fractionated Primary Production from Satellite Ocean Colour in UK Shelf Seas, Remote Sensing, 10, 1389, https://doi.org/10.3390/rs10091389, 2018.

Dall'Olmo, G., Westberry, T. K., Behrenfeld, M. J., Boss, E., and Slade, W. H.: Significant contribution of large particles to optical backscattering in the open ocean, Biogeosciences, 6, 947–967, https://doi.org/10.5194/bg-6-947-2009, 2009.

Deppeler, S. L. and Davidson, A. T.: Southern Ocean phytoplankton in a changing climate, Frontiers in Marine Science, 4, 40, https://doi.org/10.3389/fmars.2017.00040, 2017.

Devred, E., Sathyendranath, S., Stuart, V., and Platt, T.: A three component classification of phytoplankton absorption spectra: Applications to ocean-colour data, Remote Sensing of Environment, 115, 2255–2266, https://doi.org/10.1016/j.rse.2011.04.025, 2011.

Dierssen, H. M. and Smith, R. C.: Bio-optical properties and remote sensing ocean color algorithms for Antarctic Peninsula waters, Journal of Geophysical Research: Oceans, 105, 26 301–26 312, https://doi.org/10.1029/1999JC000296, 2000.

Dorschel, B., Hehemann, L., Viquerat, S., Warnke, F., Dreutter, S., Schulze Tenberge, Y., Accettella, D., An, L., Barrios, F., Bazhenova, E. A., Black, J., Bohoyo, F., Davey, C., de Santis, L., Escutia Dotti, C., Frémand, A. C., Fretwell, P. T., Gales, J. A., Gao, J., Gasperini, L., Greenbaum, J. S., Henderson Jencks, J., Hogan, K. A., Hong, J. K., Jakobsson, M., Jensen, L., Kool, J., Larin, S., Larter, R. D., Leitchenkov, G. L., Loubrieu, B., Mackay, K., Mayer, L., Millan, R., Morlighem, M., Navidad, F., Nitsche, F.-O., Nogi, Y., Pertuisot, C., Post, A. L., Pritchard, H. D., Purser, A., Rebesco, M., Rignot, E., Roberts, J. L., Rovere, M., Ryzhov, I., Sauli, C., Schmitt, T., Silvano, A., Smith, J. E., Snaith, H., Tate, A. J., Tinto, K., Vandenbossche, P., Weatherall, P., Wintersteller, P., Yang, C., Zhang, T., and Arndt, J. E.: The International Bathymetric Chart of the Southern Ocean Version 2 (IBCSO v2), https://doi.org/10.1594/PANGAEA.937574, 2022.

Dower, K. M., Lucas, M. I., Phillips, R., Dieckmann, G., and Robinson, D. H.: Phytoplankton biomass, P–I relationships and primary production in the Weddell Sea, Antarctica, during the austral autumn, Polar Biology, 16, 41–52, https://doi.org/10.1007/BF01876828, 1996.

https://doi.org/10.5194/egusphere-2026-4398
Preprint. Discussion started: 6 August 2026

Droppo, I. G.: Filtration in Particle Size Analysis, in: Encyclopedia of Analytical Chemistry, edited by Meyers, R. A., pp. 5397–5413, John Wiley & Sons Ltd, Chichester, https://doi.org/10.1002/9780470027318.a1206, 2000.

Ferreira, A., Brito, A. C., Mendes, C. R. B., Brotas, V., Costa, R. R., Guerreiro, C. V., Sá, C., and Jackson, T.: OC4-SO: A New Chlorophyll-a Algorithm for the Western Antarctic Peninsula Using Multi-Sensor Satellite Data, Remote Sensing, 14, 1052, https://doi.org/10.3390/rs14051052, 2022.

Ferreira, A., Mendes, C. R. B., Costa, R. R., Brotas, V., Tavano, V. M., Guerreiro, C. V., Secchi, E. R., and Brito, A. C.: Climate change is associated with higher phytoplankton biomass and longer blooms in the West Antarctic Peninsula, Nature Commun ications, 15, https://doi.org/10.1038/s41467-024-50381-2, 2024.

Field, C. B., Behrenfeld, M. J., Randerson, J. T., and Falkowski, P. G.: Primary production of the biosphere: integrating terrestrial and oceanic components, Science, 281, 237–240, https://doi.org/10.1126/science.281.5374.237, 1998.

Flombaum, P., Gallegos, J. L., Gordillo, R. A., Rincón, J., Zabala, L. L., Jiao, N., Karl, D. M., Li, W. K. W., Lomas, M. W., Veneziano, D., Vera, C. S., Vrén, D., and Martiny, A. C.: Present and future global distributions of the marine Cyanobacteria *Prochlorococcus* and *Synechococcus*, Proceedings of the National Academy of Sciences, 110, 9824–9829, https://doi.org/10.1073/pnas.1307701110, 2013.

Flynn, R. F., Haraguchi, L., McQuaid, J., Burger, J. M., Lunga, P. M., Stirnimann, L., Samanta, S., Roychoudhury, A., and Fawcett, S. E.: Nanoplankton: The dominant vector for carbon export across the Atlantic Southern Ocean in spring, Science Advances, 9, eadi3059, https://doi.org/10.1126/sciadv.adi3059, 2023.

Froneman, P. W., Pakhomov, E. A., and Balarin, M. G.: Size-fractionated phytoplankton biomass, production and biogenic carbon flux in the eastern Atlantic sector of the Southern Ocean in late austral summer 1997–1998, Deep-Sea Research Part II: Topical Studies in Oceanography, 51, 2715–2729, https://doi.org/10.1016/j.dsr2.2002.09.001, 2004.

Fuchs, H. L. and Franks, P. J. S.: Plankton community properties determined by nutrients and size-selective feeding, Marine Ecology Progress Series, 413, 1–15, https://doi.org/10.3354/meps08716, 2010.

Garcia, C. A. E., Garcia, V. M. T., and McClain, C. R.: Evaluation of SeaWiFS chlorophyll algorithms in the Southwestern Atlantic and Southern Oceans, Remote Sensing of Environment, 95, 125–137, https://doi.org/10.1016/j.rse.2004.12.006, 2005.

García-Muñoz, C., Sobrino, C., Lubián, L. M., García, C. M., Martínez-García, S., and Sangrà, P.: Factors controlling phytoplankton physiological state around the South Shetland Islands (Antarctica), Marine Ecology Progress Series, 498, 55–71, https://doi.org/10.3354/meps10616, 2014.

Garibotti, I. A., Vernet, M., Kozlowski, W. A., and Ferrario, M. E.: Composition and biomass of phytoplankton assemblages in coastal Antarctic waters: A comparison of chemotaxonomic and microscopic analyses, Marine Ecology Progress Series, 247, 27–42, https://doi.org/10.3354/meps247027, 2003.

GCOS: Systematic observation requirements from satellite-based data products for climate, Tech. rep., World Meteorological Organisation (WMO), 7 bis, avenue de la Paix, CH-1211 Geneva 2, Switzerland., 2011.

Gittings, J. A., Brewin, R. J. W., Raitsos, D. E., Kheireddine, M., Ouhssain, M., Jones, B. H., and Hoteit, I.: Remotely Sensing Phytoplankton Size Structure in the Red Sea, Remote Sensing of Environment, 234, 111 387, https://doi.org/10.1016/j.rse.2019.111387, 2019.

Gittings, J. A., Livanou, E., Sun, X., Brewin, R. J. W., Psarra, S., Mandalakis, M., Peltekis, A., Di Cicco, A., Brando, V. E., and Raitsos, D. E.: Remotely Sensing Phytoplankton Size Structure in the Mediterranean Sea: Insights from In Situ Data and Temperature-Corrected Abundance-Based Models, Remote Sensing, 17, 2362, https://doi.org/10.3390/rs17142362, 2025.

Goericke, R.: Top-down control of phytoplankton biomass and community structure in the monsoonal Arabian Sea, Limnology and Oceanography, 47, 1307–1323, https://doi.org/https://doi.org/10.4319/lo.2002.47.5.1307, 2002.

https://doi.org/10.5194/egusphere-2026-4398
Preprint. Discussion started: 6 August 2026

Gonçalves-Araujo, R., de Souza, M. S., Tavano, V. M., and Garcia, C. A. E.: Influence of oceanographic features on spatial and interannual variability of phytoplankton in the Bransfield Strait, Antarctica, Journal of Marine Systems, 142, 1–15, https://doi.org/10.1016/j.jmarsys.2014.09.007, 2015.

Guidi, L., Stemmann, L., Jackson, G. A., Ibanez, F., Claustre, H., Legendre, L., Picheral, M., and Gorskya, G.: Effects of phytoplankton community on production, size and export of large aggregates: A world-ocean analysis, Limnology and Oceanography, 54, 1951–1963, https://doi.org/10.4319/lo.2009.54.6.1951, 2009.

Hayward, A., W. S. C. D., Law, C. S., Wongpan, P., Guti'errez-Rodriguez, A., and Pinkerton, M. H.: Antarctic phytoplankton communities restructure under shifting sea-ice regimes, Nature Climate Change, 15, 889–896, https://doi.org/10.1038/s41558-025-02379-x, 2025.

Haëntjens, N., Boss, E., and Talley, L.: Revisiting Ocean Color algorithms for chlorophyll a and particulate organic carbon in the Southern Ocean using biogeochemical floats, Journal of Geophysical Research: Oceans, 122, 6583–6593, https://doi.org/10.1002/2017JC012844, 2017.

Hewes, C. D.: Cell size of Antarctic phytoplankton as a biogeochemical condition, Antarctic Science, 21, 457–470, https://doi.org/10.1017/S0954102009990125, 2009.

Heywood, K. J. and Bell, T.: RRS Sir David Attenborough cruise SD035, 17 January–08 March 2024. PICCOLO cruise report, Tech. Rep. SD035 cruise report, British Oceanographic Data Centre (BODC), https://www.bodc.ac.uk/resources/inventories/cruise_inventory/reports/sd035.pdf, 2024.

IOCCG: Phytoplankton Functional Types from Space., Tech. rep., Sathyendranath, S. (e.d.), Reports of the International Ocean-Colour Coordinating Group, No. 15, IOCCG, Dartmouth, Canada., 2014.

Jacques, G. and Panouse, M.: Biomass and composition of size fractionated phytoplankton in the Weddell-Scotia Confluence area, Polar Biology, 11, 315–328, https://doi.org/10.1007/BF00239024, 1991.

Jochem, F. J., Mathot, S., and Quéguiner, B.: Size-fractionated primary production in the open Southern Ocean in austral spring, Polar Biology, 15, 381–392, https://doi.org/10.1007/BF00239714, 1995.

Johnson, R. S., Strutton, P. G., Wright, S. W., McMinn, A., and Meiners, K. M.: Three improved satellite chlorophyll algorithms for the Southern Ocean, Journal of Geophysical Research: Oceans, 118, 3694–3703, https://doi.org/10.1002/jgrc.20270, 2013.

Kiørboe, T.: How zooplankton feed: mechanisms, traits and trade-offs, Biological Reviews, 86, 311–339, https://doi.org/10.1111/j.1469-185X.2010.00148.x, 2011.

Kishi, M. J., Kashiwai, M., Ware, D. M., Megrey, B. A., Eslinger, D. L., Werner, F. E., Noguchi-Aita, M., Azumaya, T., Fujii, M., Hashimoto, S., Huang, D. J., Iizumi, H., Ishida, Y., Kang, S., Kantakov, G. A., Kim, H. C., Komatsu, K., Navrotsky, V. V., Smith, S. L., Tadokoro, K., Tsuda, A., Yamamura, O., Yamanaka, Y., Yokouchi, K., Yoshie, N., Zhang, J., Zuenko, Y. I., and Zvalinsky, V. I.: NEMURO–a lower trophic level model for the North Pacific marine ecosystem, Ecological Modelling, 202, 12–25, https://doi.org/10.1016/j.ecolmodel.2006.08.021, 2007.

Knefelkamp, B., Carstens, K., and Wiltshire, K. H.: Comparison of Different Filter Types on Chlorophyll-*a* Retention and Nutrient Measurements, Journal of Experimental Marine Biology and Ecology, 345, 61–70, https://doi.org/10.1016/j.jembe.2007.01.008, 2007.

Korb, R. E., Whitehouse, M. J., Atkinson, A., and Thorpe, S. E.: Magnitude and maintenance of the phytoplankton bloom at South Georgia: a naturally iron-replete environment, Marine Ecology Progress Series, 368, 75–91, https://doi.org/10.3354/meps07525, 2008.

Korb, R. E., Whitehouse, M. J., Ward, P., Gordon, M., Venables, H. J., and Poulton, A. J.: Regional and seasonal differences in microplankton biomass, productivity, and structure across the Scotia Sea: Implications for the export of biogenic carbon, Deep Sea Research Part II: Topical Studies in Oceanography, 59, 67–77, https://doi.org/10.1016/j.dsr2.2011.06.006, 2012.

https://doi.org/10.5194/egusphere-2026-4398
Preprint. Discussion started: 6 August 2026

Krumhardt, K. M., Landrum, L., Şen, B., DuVivier, A. K., Levy, M. N., Nissen, C., Holland, M. M., and Jenouvrier, S.: Emergent climate change signals within Antarctic sea ice and associated ecosystems, Nature Climate Change, 16, 364–371, https://doi.org/10.1038/s41558-026-02356-8, 2026.

Lamont, T., Barlow, R. G., and Brewin, R. J. W.: Variations in remotely-sensed phytoplankton size structure of a cyclonic eddy in the Southwest Indian Ocean, Remote Sensing, 10, 1143, https://doi.org/10.3390/rs10071143, 2018a.

Lamont, T., Brewin, R. J. W., and Barlow, R.: Seasonal Variation in Remotely-Sensed Phytoplankton Size Structure Around Southern Africa, Remote Sensing of Environment, 204, 617–631, https://doi.org/10.1016/j.rse.2017.09.038, 2018b.

Lancelot, C., Mathot, S., Veth, C., and de Baar, H. J. W.: Factors controlling phytoplankton ice-edge blooms in the marginal ice-zone of the northwestern Weddell Sea during sea ice retreat 1988: Field observations and mathematical modelling, Polar Biology, 13, 377–387, https://doi.org/10.1007/BF01681979, 1993.

Lange, P. K., Brewin, R. J. W., Dall'Olmo, G., Tarran, G. A., Sathyendranath, S., Zubkov, M., and Bouman, H. A.: Scratching Beneath the Surface: A Model to Predict the Vertical Distribution of *Prochlorococcus* Using Remote Sensing, Remote Sensing, 10, 847, https://doi.org/10.3390/rs10060847, 2018.

Lange, P. K., Werdell, P. J., Erickson, Z. K., Dall'Olmo, G., Brewin, R. J. W., Zubkov, M. V., Tarran, G. A., Bouman, H. A., Slade, W. H., Craig, S. E., Poulton, N. J., Bracher, A., Lomas, M. W., and Cetinić, I.: Radiometric approach for the detection of picophytoplankton assemblages across oceanic fronts, Optics Express, 28, 25 682–25 705, https://doi.org/10.1364/OE.398127, 2020.

Laubscher, R. K., Perissinotto, R., and McQuaid, C. D.: Phytoplankton production and biomass at frontal zones in the Atlantic sector of the Southern Ocean, Polar Biology, 13, 471–481, https://doi.org/10.1007/BF00233138, 1993.

Laws, E. A. and Bannister, T. T.: Nutrient- and light-limited growth of *Thalassiosira fluviatilis* in continuous culture, with implications for phytoplankton growth in the ocean, Limnology and Oceanography, 25, 457–473, https://doi.org/10.4319/lo.1980.25.3.0457, 1980.

Legendre, L. and LeFevre, J.: From individual plankton cells to pelagic marine ecosystems and to global biogeochemical cycles, in: Particle Analysis in Oceanography, edited by Demers, S., pp. 261–300, Springer, Berlin, 1991.

Li, J., Antoine, D., and Huot, Y.: Bio-optical variability of particulate matter in the Southern Ocean, Frontiers in Marine Science, 11, https://doi.org/10.3389/fmars.2024.1466037, 2024.

Li, J., Antoine, D., and Huot, Y.: Unexpected quasi-independence of coloured dissolved organic matter absorption from chlorophyll-a concentration in the Southern Ocean, Biogeosciences, 23, 3073–3090, https://doi.org/10.5194/bg-23-3073-2026, 2026.

Lin, J., Cao, W., Wang, G., and Hu, S.: Satellite-observed variability of phytoplankton size classes associated with a cold eddy in the South China Sea, Marine Pollution Bulletin, 83, 190–197, https://doi.org/10.1016/j.marpolbul.2014.03.052, 2014.

Lin, J., Dall'Olmo, G., Tilstone, G. H., Brewin, R. J. W., Vabson, V., Ansko, I., Evers-King, H., Casal, T., and Donlon, C.: Derivation of uncertainty budgets for continuous above-water radiometric measurements along an Atlantic Meridional Transect, Optics Express, 30, 45 648–45 675, https://doi.org/10.1364/OE.470994, 2022.

Logan, B. E.: Theoretical Analysis of Size Distributions Determined with Screens and Filters, Limnology and Oceanography, 38, 372–381, https://doi.org/10.4319/lo.1993.38.2.0372, 1993.

Logan, B. E., Passow, U., and Alldredge, A. L.: Variable Retention of Diatoms on Screens during Size Separations, Limnology and Oceanography, 39, 390–395, https://doi.org/10.4319/lo.1994.39.2.0390, 1994.

Longhurst, A., Sathyendranath, S., Platt, T., and Caverhill, C.: An estimate of global primary production in the ocean from satellite radiometer data, Journal of Plankton Research, 17, 1245–1271, https://doi.org/10.1093/plankt/17.6.1245, 1995.

https://doi.org/10.5194/egusphere-2026-4398
Preprint. Discussion started: 6 August 2026

López-Urrutia, A. and Morán, X. A. G.: Temperature affects the size-structure of phytoplankton communities in the ocean, Limnology and Oceanography, 60, 733–738, https://doi.org/https://doi.org/10.1002/lno.10049, 2015.

Maloney, C. L. and Field, J. G.: The size-based dynamics of plankton food webs. I. A simulation model of carbon and nitrogen flows, Journal of Plankton Research, 13, 1003–1038, https://doi.org/10.1093/plankt/13.5.1003, 1991.

Marañón, E.: Phytoplankton size structure, in: Encyclopedia of Ocean Sciences, edited by Steele, J. H., Turekian, K., and Thorpe, S. A., Academic Press, Oxford, 2009.

Marañón, E.: Cell size as a key determinant of phytoplankton metabolism and community structure, Annual Review of Marine Science, 7, 241–264, https://doi.org/10.1146/annurev-marine-010814-015955, 2015.

Marañón, E., Cermeño, P., López-Sandoval, D. C., Rodríguez-Ramos, T., Sobrino, C., Huete-Ortega, M., Blanco, J. M., and Rodríguez, J.: Unimodal size scaling of phytoplankton growth and the size dependence of nutrient uptake and use, Ecology Letters, 16, 371–379, https://doi.org/10.1111/ele.12052, 2013.

Marinov, I., Doney, S. C., and Lima, I. D.: Response of ocean phytoplankton community structure to climate change over the 21st century: partitioning the effects of nutrients, temperature and light, Biogeosciences, 7, 3941–3959, https://doi.org/10.5194/bgd-7-4565-2010, 2010.

Meier, W. N., Fetterer, F., Windnagel, A. K., Stewart, J. S., and Stafford, T.: NOAA/NSIDC Climate Data Record of Passive Microwave Sea Ice Concentration, Version 6, https://doi.org/10.7265/b18jz797, 2024.

Mendes, C. R. B., Costa, R. R., Ferreira, A., Jesus, B., Tavano, V. M., Dotto, T. S., Leal, M. C., Kerr, R., Islabão, C. A., Franco, A. O. R., Mata, M. M., Garcia, C. A. E., and Secchi, E. R.: Cryptophytes: An emerging algal group in the rapidly changing Antarctic Peninsula marine environments, Global Change Biology, 29, 1791–1808, https://doi.org/10.1111/gcb.16602, 2023.

Meyer, M. G., Brewin, R. J. W., Sun, X., Manno, C., Atherden, F., Kramer, S. J., Dall'Olmo, G., and Heywood, K. J.: Spatial patterns in phytoplankton community composition and their influence on carbon export on the northwest Weddell Sea continental shelf, ESS Open Archive, https://doi.org/10.22541/essoar.15002170/v1, 2026a.

Meyer, M. G., Sun, X., Brewin, R. J. W., and Dall'Olmo, G.: High performance liquid chromatography samples from water, ice and interfacial samples collected during RRS Sir David Attenborough cruise SD035 in the Southern Ocean in February 2024 as part of the PICCOLO project, NERC EDS British Oceanographic Data Centre, National Oceanography Centre, https://doi.org/10.5285/4d5d158b-3cf9-ad21-e063-7086abc01540, 2026b.

Mitchell, B. G.: Predictive bio-optical relationships for polar oceans and marginal ice zones, Journal of Marine Systems, 3, 91–105, https://doi.org/10.1016/0924-7963(92)90032-4, 1992.

Mobley, C. D.: Estimation of the remote-sensing reflectance from above-surface measurements, Applied Optics, 38, 7442–7455, https://doi.org/10.1364/AO.38.007442, 1999.

Montes-Hugo, M. A., Vernet, M., Smith, R. C., and Carder, K.: Phytoplankton size-structure on the western shelf of the Antarctic Peninsula: a remote-sensing approach, International Journal of Remote Sensing, 29, 801–829, https://doi.org/10.1080/01431160701297615, 2008.

Moutier, W., Thomalla, S. J., Bernard, S., Wind, G., Ryan-Keogh, T. J., and Smith, M. E.: Evaluation of Chlorophyll-a and POC MODIS Aqua Products in the Southern Ocean, Remote Sensing, 11, 1793, https://doi.org/10.3390/rs11151793, 2019.

Mura, M. P., Satta, M. P., and Agustı, S.: Water-mass influences on summer Antarctic phytoplankton biomass and community structure, Polar Biology, 15, 15–20, https://doi.org/10.1007/BF00236119, 1995.

Naughten, K. A., Holland, P. R., and De Rydt, J.: Unavoidable future increase in West Antarctic ice-shelf melting over the twenty-first century, Nature Climate Change, 13, 1222–1228, https://doi.org/10.1038/s41558-023-01818-x, 2023.

https://doi.org/10.5194/egusphere-2026-4398
Preprint. Discussion started: 6 August 2026

Nowicki, M., DeVries, T., and Siegel, D.: Quantifying the Carbon Export and Sequestration Pathways of the Ocean's Biological Carbon Pump, Global Biogeochemical Cycles, 36, e2021GB007 083, https://doi.org/10.1029/2021GB007083, 2022.

O'Reilly, J. E. and Werdell, P. J.: Chlorophyll algorithms for ocean color sensors – OC4, OC5 & OC6, Remote Sensing of Environment, 229, 32–47, https://doi.org/10.1016/j.rse.2019.04.021, 2019.

O'Reilly, J. E., Maritorena, S., Siegel, D., O'Brien, M. C., Toole, D.and Mitchell, B. G., Kahru, M., Chavez, F. P., Strutton, P., Cota, G., Hooker, S. B., McClain, C. R., Carder, K. L., Muller-Karger, F., Harding, L., Magnuson, A., Phinney, D., Moore, G. F., Aiken, J., Arrigo, K. R., Letelier, R., and Culver, M.: Ocean color chlorophyll a algorithms for SeaWiFS, OC2, and OC4:, Tech. rep., In: Hooker, S. B., Firestone, E. R. (Eds.), SeaWiFS Postlaunch Technical Report Series. Vol. 11. SeaWiFS Postlaunch Calibration and Validation Analyses, Part 3. NASA, Goddard Space Flight Center, Greenbelt, Maryland. 9-23., 2000.

Organelli, E., Dall'Olmo, G., Brewin, R. J. W., Tarran, G. A., Boss, E., and Bricaud, A.: The open-ocean missing backscattering is in the structural complexity of particles, Nature Communications, 9, 1–11, https://doi.org/10.1038/s41467-018-07814-6, 2018.

Ortega-Retuerta, E., Siegel, D. A., Nelson, N. B., Duarte, C. M., and Reche, I.: Observations of chromophoric dissolved and detrital organic matter distribution using remote sensing in the Southern Ocean: Validation, dynamics and regulation, Journal of Marine Systems, 82, 295–303, https://doi.org/10.1016/j.jmarsys.2010.06.004, 2010.

Parsons, T. R. and Lalli, C. M.: Jellyfish populations explosions: Revisiting a hypothesis of possible causes, La Mer, 40, 111–121, 2002.

Platt, T. and Denman, K. L.: The structure of pelagic marine ecosystems, Rapp. P.-v. Réun. Cons. perm. int. Explor. Mer, pp. 60–65, 1978.

Platt, T. and Sathyendranath, S.: Ecological indicators for the pelagic zone of the ocean from remote sensing, Remote Sensing of Environment, 112, 3426–3436, https://doi.org/10.1016/j.rse.2007.10.016, 2008.

Purich, A. and Doddridge, E. W.: Record low Antarctic sea ice coverage indicates a new sea ice state, Communications Earth & Environment, 4, 314, https://doi.org/10.1038/s43247-023-00961-9, 2023.

Reynolds, R. A., Stramski, D., and Mitchell, B. G.: A chlorophyll-dependent semianalytical reflectance model derived from field measurements of absorption and backscattering coefficients within the Southern Ocean, Journal of Geophysical Research: Oceans, 106, 7125–7138, https://doi.org/10.1029/1999JC000311, 2001.

Robinson, C. M., Huot, Y., Schuback, N., Ryan-Keogh, T. J., Thomalla, S. J., and Antoine, D.: High latitude Southern Ocean phytoplankton have distinctive bio-optical properties, Optics Express, 29, 21 084–21 112, https://doi.org/10.1364/OE.426737, 2021.

Sahay, A., Ali, S. M., Gupta, A., and Goes, J. I.: Ocean Color Satellite Determinations of Phytoplankton Size Class in the Arabian Sea During the Winter Monsoon, Remote Sensing of Environment, 198, 286–296, https://doi.org/10.1016/j.rse.2017.06.017, 2017.

Salyuk, P. A., Glukhovets, D. I., Latushkin, A. A., Kalinina, O. Y., Shtraikhert, E. A., Sapozhnikov, P. V., Mosharov, S. A., Stepochkin, I. E., Lipinskaya, N. A., Gorbov, M. I., and Klimenko, S. K.: Extreme underestimation of satellite-derived chlorophyll-a concentration in the northwestern Weddell Sea during a phytoplankton bloom and its reasons, Journal of Marine Systems, 252, 104 159, https://doi.org/10.1016/j.jmarsys.2025.104159, 2025.

Sammartino, M., Di Cicco, A., Marullo, S., and Santoleri, R.: Spatio-temporal variability of micro-, nano- and pico-phytoplankton in the Mediterranean Sea from satellite ocean colour data of SeaWiFS, Ocean Sciences, 11, 759–778, https://doi.org/10.5194/os-11-759-2015, 2015.

Sanders, R., Henson, S. A., Koski, M., Christina, L., Painter, S. C., Poulton, A. J., Riley, J., Salihoglu, B., Visser, A., Yool, A., and Bellerby, R.: The biological carbon pump in the North Atlantic, Progress in Oceanography, 129, 200–218, https://doi.org/10.1016/j.pocean.2014.05.005, 2014.

https://doi.org/10.5194/egusphere-2026-4398
Preprint. Discussion started: 6 August 2026

Sathyendranath, S., Brewin, R. J. W., Brockmann, C., Brotas, V., Calton, B., Chuprin, A., Cipollini, P., Couto, A. B., Dingle, J., Doerffer, R., Donlon, C., Dowell, M., Farman, A., Grant, M., Groom, S., Horseman, A., Jackson, T., Krasemann, H., Lavender, S., Martinez-Vicente, V., Mazeran, C., Mélin, F., Moore, T. S., Müller, D., Regner, P., Roy, S., Steele, C. J., Steinmetz, F., Swinton, J., Taberner, M., Thompson, A., Valente, A., Zühlke, M., Brando, V. E., Feng, H., Feldman, G., Franz, B. A., Frouin, R., Gould, R. W., Hooker, S. B., Kahru, M., Kratzer, S., Mitchell, B. G., Muller-Karger, F. E., Sosik, H. M., Voss, K., Werdell, J., and Platt, T.: An Ocean-Colour Time Series for Use in Climate Studies: The Experience of the Ocean-Colour Climate Change Initiative (OC-CCI), Sensors, 19, 4285, https://doi.org/10.3390/s19194285, 2019.

Sathyendranath, S., Brewin, R. J. W., Jönsson, B. F., Ciavatta, S., Jackson, T., Kulk, G., Vicente, V. M., and Platt, T.: Ocean biology from space, Survey in Geophysics, 44, 1287–1308, https://doi.org/10.1007/s10712-023-09805-9, 2023.

Savidge, G., Harbour, D. S., Gilpin, L. C., and Boyd, P. W.: Phytoplankton distributions and production in the Bellingshausen Sea, austral spring 1992, Deep-Sea Research Part II: Topical Studies in Oceanography, 42, 1201–1224, https://doi.org/10.1016/0967-0645(95)00062-U, 1995.

Schmidt, K. and Atkinson, A.: Feeding and food processing in Antarctic krill (*Euphausia superba* Dana), in: Biology and Ecology of Antarctic Krill, edited by Siegel, V., Advances in Polar Ecology, chap. 5, Springer, https://doi.org/10.1007/978-3-319-29279-3_5, 2016.

Sheldon, R. W.: Size separation of marine seston by membrane and glass-fiber filters, Limnology and Oceanography, 17, 494–498, https://doi.org/10.4319/lo.1972.17.3.0494, 1972.

Sheldon, R. W., Prakash, A., and Sutcliffe Jr, W. H.: The size distribution of particles in the ocean, Limnology and Oceanography, 17, 327–340, https://doi.org/10.4319/lo.1972.17.3.0327, 1972.

Sieburth, J. M., Smetacek, V., and Lenz, J.: Pelagic ecosystem structure: Heterotrophic compartments of the plankton and their relationship to plankton size fractions, Limnology and Oceanography, 23, 1256–1263, https://doi.org/10.4319/lo.1978.23.6.1256, 1978.

Siegel, D. A., Buesseler, K. O., Doney, S. C., Sailley, S. F., Behrenfeld, M. J., and Boyd, P. W.: Global assessment of ocean carbon export by combining satellite observations and food-web models, Global Biogeochemical Cycles, 28, 181–196, https://doi.org/10.1002/2013gb004743, 2014.

Smith, R. C., Baker, K. S., Fraser, W. R., Hofmann, E. E., Karl, D. M., Klinck, J. M., Quetin, L. B., Prezelin, B. B., Ross, R. M., Trivelpiece, W. Z., and Vernet, M.: The Palmer LTER: A Long-Term Ecological Research Program at Palmer Station, Antarctica, Oceanography, 8, 77–86, 1995.

Soja-Woźniak, M., Holtrop, T., Woutersen, S., van der Woerd, H. J. an Lund-Hansen, L. C., and Huisman, J.: Loss of sea ice alters light spectra for aquatic photosynthesis, Nature Communications, 16, 4059, https://doi.org/10.1038/s41467-025-59386-x, 2025.

Sun, X.and Brewin, R. J. W., Sathyendranath, S., Dall'Olmo, G., Airs, R., Barlow, R., Bracher, A., Brotas, V., Kheireddine, M., Lamont, T., Marañón, E., Morán, X. A. G., Raitsos, D. E., Shen, F., and Tilstone, G. H.: Coupling ecological concepts with an ocean-colour model: Phytoplankton size structure, Remote Sensing of Environment, 285, 113 415, https://doi.org/10.1016/j.rse.2022.113415, 2023.

Sun, X., Shen, F., Brewin, R. J. W., Liu, D., and Tang, R.: Twenty-Year Variations in Satellite-Derived Chlorophyll-a and Phytoplankton Size in the Bohai Sea and Yellow Sea, Journal of Geophysical Research: Oceans, 124, 8887–8912, https://doi.org/10.1029/2019JC015552, 2019.

Sun, X., Brewin, R. J. W., Dall'Olmo, G., Pitarch, J., Bell, T., Wilkinson, B., Raitsos, D. E., van der Woerd, H. J., and Sathyendranath, S.: Unifying theories on the Southern Ocean bio-optical anomaly, Research Square, https://doi.org/10.21203/rs.3.rs-7906673/v1, 2025a.

https://doi.org/10.5194/egusphere-2026-4398
Preprint. Discussion started: 6 August 2026

Sun, X., Brewin, R. J. W., Sathyendranath, S., Dall'Olmo, G., Antoine, D., Barlow, R., Bracher, A., Kheireddine, M., Li, M., Raitsos, D. E., Shen, F., Tilstone, G. H., and Vellucci, V.: Coupling ecological concepts with an ocean-colour model: Parameterisation and forward modelling, Remote Sensing of Environment, 316, 114 487, https://doi.org/10.1016/j.rse.2024.114487, 2025b.

Szeto, M., Werdell, P. J., Moore, T. S., and Campbell, J. W.: Are the world's oceans optically different?, Journal of Geophysical Research: Oceans, 116, https://doi.org/10.1029/2011JC007230, 2011.

Tarran, G. A.: Phytoplankton and bacterioplankton abundance within and below the sea-ice measured using flow cytometry during PICCOLO research cruise SD035 to the Southern Ocean in Feb–Mar 2024, https://doi.org/10.5285/487f129d-a40a-305b-e063-7086abc0ac13, 2026.

Tilstone, G., Lange, P. K., Misra, A., Brewin, R. J. W., and Cain, T.: Micro-phytoplankton photosynthesis, primary production and potential export production in the Atlantic Ocean., Progress in Oceanography, 158, 109–129, https://doi.org/10.1016/j.pocean.2017.01.006, 2017.

Uitz, J., Claustre, H., Morel, A., and Hooker, S. B.: Vertical distribution of phytoplankton communities in open ocean: an assessment based on surface chlorophyll, Journal of Geophysical Research, 111, C08 005, https://doi.org/10.1029/2005JC003207, 2006.

Uitz, J., Huot, Y., Bruyant, F., Babin, M., and Claustre, H.: Relating phytoplankton photophysiological properties to community structure on large scales, Limnology and Oceanography, 53, 614–630, https://doi.org/10.4319/lo.2008.53.2.0614, 2008.

Uitz, J., Claustre, H., Brian Griffiths, F., Ras, J., Garcia, N., and Sandroni, V.: A phytoplankton class-specific primary production model applied to the Kerguelen Islands region (Southern Ocean), Deep-Sea Research I, 56, 541–560, https://doi.org/10.1016/j.dsr.2008.11.006, 2009.

Van Heukelem, L. and Thomas, C. S.: Computer-assisted high-performance liquid chromatography method development with applications to the isolation and analysis of phytoplankton pigments, Journal of Chromatography A, 910, 31–49, https://doi.org/10.1016/S0378-4347(00)00603-4, 2001.

Venables, H. J., Meredith, M. P., Hendry, K. R., ten Hoopen, P., Peat, H., Chapman, A., Beaumont, J., Piper, R., Miller, A. J., Mann, P., Rossetti, H., Massey, A., Souster, T., Reeves, S., Fenton, M., Heiser, S., Pountney, S., Reed, S., Waring, Z., Clark, M., Bolton, E., Mathews, R., London, H., Clement, A., Stuart, E., Reichardt, A., Brandon, M., Leng, M., Arrowsmith, C., Annett, A., Henley, S. F., and Clarke, A.: Sustained year-round oceanographic measurements from Rothera Research Station, Antarctica, 1997–2017, Scientific Data, 10, https://doi.org/10.1038/s41597-023-02172-5, 2023.

Vernet, M., Sines, K., Chakos, D., Cefarelli, A. O., and Ekern, L.: Impacts on phytoplankton dynamics by free-drifting icebergs in the northwestern Weddell Sea, Deep-Sea Research Part II: Topical Studies in Oceanography, 58, 1422–1435, https://doi.org/10.1016/j.dsr2.2010.11.022, 2011.

Vidussi, F., Claustre, H., Manca, B. B., Luchetta, A., and Marty, J. C.: Phytoplankton pigment distribution in relation to upper thermocline circulation in the eastern Mediterranean Sea during winter, Journal of Geophysical Research, 106, 19,939–19,956, https://doi.org/10.1029/1999JC000308, 2001.

Viljoen, J. J., Cloete, R., Philibert, R., Hayward, A., Valk, O., Loock, J. C., van Horsten, N. R., Planquette, H., Bucciarelli, E., Sarthou, G., Roychoudhury, A. N., and Fietz, S.: Winter Dynamics of Phytoplankton and Micronutrients in the Southern Ocean, Journal of Geophysical Research: Oceans, 130, e2025JC022 431, https://doi.org/https://doi.org/10.1029/2025JC022431, 2025.

von Bröckel, K.: Primary production data from the south-eastern Weddell Sea, Polar Biology, 4, 75–80, https://doi.org/10.1007/BF00442903, 1985.

Ward, B. A.: Temperature-Correlated Changes in Phytoplankton Community Structure Are Restricted to Polar Waters, PLoS ONE, 10, e0135 581, https://doi.org/10.1371/journal.pone.0135581, 2015.

https://doi.org/10.5194/egusphere-2026-4398
Preprint. Discussion started: 6 August 2026

Ward, B. A.: How phytoplankton compete for nutrients despite vast intercellular separation, ISME Communications, 4, ycae003, https://doi.org/10.1093/ismeco/ycae003, 2024.

Ward, B. A., Dutkiewicz, S., Jahn, O., and Follows, M. J.: A size-structured food-web model for the global ocean, Limnology and Oceanography, 57, 1877–1891, https://doi.org/10.4319/lo.2012.57.6.1877, 2012.

Ward, P., Shreeve, R., Atkinson, A., Korb, B., Whitehouse, M., Thorpe, S., Pond, D., and Cunningham, N.: Plankton community structure and variability in the Scotia Sea: austral summer 2003, Marine Ecology Progress Series, 309, 75–91, https://doi.org/10.3354/meps309075, 2006.

Weber, L. H. and El-Sayed, S. Z.: Contributions of the net, nano- and picoplankton to the phytoplankton standing crop and primary productivity in the Southern Ocean, Journal of Plankton Research, 9, 973–994, https://doi.org/10.1093/plankt/9.5.973, 1987.

Werdell, P. J. and Bailey, S. W.: An improved in-situ bio-optical data set for ocean colour algorithm development and satellite data production validation, Remote Sensing Environment, 98, 122–140, https://doi.org/10.1016/j.rse.2005.07.001, 2005.

Wilkinson, B.: Chlorophyll-a samples collected in the Southern Ocean on cruise SD035 in January–March 2024 as part of PICCOLO, NERC EDS British Oceanographic Data Centre, National Oceanography Centre, https://doi.org/10.5285/4f7aed48-816a-d8cf-e063-7086abc055b4, 2026.

Wille, J. D., Alexander, S. P., Amory, C., Baiman, R., Barthélemy, L., Bergstrom, D. M., Berne, A., Binder, H., Blanchet, J., Bozkurt, D., and Bracegirdle, T. J.: The extraordinary March 2022 East Antarctica "heat" wave. Part I: observations and meteorological drivers, Journal of Climate, 37, 757–778, https://doi.org/10.1175/JCLI-D-23-0175.1, 2024.

Xiuren, N., Zilin, L., Genhai, Z., and Junxian, S.: Size-fractionated biomass and productivity of phytoplankton and particulate organic carbon in the Southern Ocean, Polar Biology, 16, 1–11, https://doi.org/10.1007/BF02388729, 1996.